이학박사 학위논문

Laplace Transform Method and Its Applications for Weather Derivatives

라플라스 변환 방법과 날씨파생상품에서의 응용

2013 년 8 월

서울대학교 대학원

수리과학부

김 지 운

Abstract

Laplace Transform Method and Its Applications for Weather Derivatives

Jiwoon Kim
Department of Mathematical Sciences
The Graduate School
Seoul National University

In this thesis we deal with the most efficient methods for numerical Laplace inversion and analyze the effect of roundoff errors. There are three issues in the control of numerical Laplace inversion: the choice of contour, its parameterization and numerical quadrature. We extend roundoff error control to the case of numerical inversion for hyperbolic contour. Also in order to examine the effect of roundoff error, computation is carried out both in double-precision and multi-precision, the latter which provides better understanding of the numerical Laplace inversion algorithms.

We analyze temperature data for Seoul based on a well defined daily average temperature and consider related weather derivatives. The temperature data exhibit some quite distinctive features, compared to other cities that have been considered before. Due to these characteristics, seasonal variance and oscillation in Seoul is more apparent in winter and less evident in summer than in the other cities. We construct a deterministic model for the average temperature and then simulate future weather patterns, before pricing various weather derivative options and calculating the market price of risk.

And Laplace transform method is applicable for solving the partial differential equation of weather derivatives.

Keywords : Laplace transform, numerical contour integration, roundoff error, multi-precision, weather derivatives

Student Number : 2010-30084

Contents

Chapter 1

Introduction

Laplace transform method is an efficient technique which has high convergence and can be easily solved in parallel. Laplace transform method has been recently popularized and applied to solve parabolic problems [21, 22, 23, 37, 40, 41, 42, 47, 52, 53, 54]. In this thesis we first deal with numerical Laplace inversion including roundoff error analysis. We then analyze temperature data and consider related weather derivatives. Finally, Laplace transform method can be applied to solve the partial differential equation for weather derivatives.

In Chapter 2 we first review and compare the most efficient methods for numerical Laplace inversion. Several methods have been classified and interpreted as the contents related to the following issues: (i) the choice of contour & its parameterization, and (ii) infinity-to-finite interval map & numerical quadrature rule. In numerical computations the roundoff error can be a significant factor and should be considered to achieve accurate results. There are former researches to resolve the effect of roundoff error [36, 41, 52]. We extend

the roundoff error model suggested by Weideman [52] to find the modified optimal parameter for hyperbolic contour which gives great efficiency. Also computation is carried out both in double-precision and multi-precision. An multi-precision arithmetic environment which is developed by Fujiwara [19] was set and it gives us more accurate results, compared to double-precision in numerical results. From our examples, we conclude that the method which hyperbola is used as contour is more efficient than the case of using parabola or cotangent contour. This chapter is from a preprint with Dongwoo Sheen [30, 31].

In Chapter 3 we consider weather derivatives which have been popularized to provide against uncertain climatic change. With the rapid growth of weather-related market, the pricing of weather derivatives have been studied by many researchers [2, 3, 4, 5, 6, 7, 9, 11, 25, 27, 55]. However there are few investigations reported on weather derivatives and their pricing for Asian countries, including Korea. We have extended the temperature model suggested by Alaton *et al.* (2002) and Benth *et al.* (2007) to evaluate option prices for the temperature at Seoul. Using a deterministic model, we price put and call options that are based on the temperature derivatives. Since no weather derivatives market exists in Seoul, we consider the market price of risk (MPR) using the Korea Composite Stock Price Index (KOSPI). This part is based on the paper [32]. Finally, we apply Laplace transform method to solve the partial differential equation for weather-related derivatives.

Chapter 2

Laplace Transform Methods

2.1 Introduction

Let us start to consider the evolution problem:

$$u_t + Au = f(t), \quad \text{for} \quad t > 0, \quad \text{with } u(0) = u_0, \tag{2.1}$$

where u_0 and $f(t)$ are given and A is an elliptic operator in a Banach space X. We assume that the spectrum $\sigma(A)$ of A satisfies

$$\sigma(A) \subset \Sigma_\delta := \{z \in \mathbb{C} : |\arg z| \leq \delta, z \neq 0, \delta \in (0, \pi/2)\}, \tag{2.2}$$

and the resolvent $(zI + A)^{-1}$ of $-A$ fulfils

$$\| (zI + A)^{-1} \| \leq M(1 + |z|)^{-1} \quad \text{for} \quad z \in \Sigma_{\pi-\delta} \cup B, \tag{2.3}$$

where B is a small neighborhood of the origin and $\delta \in (0, \pi)$.

Due to Bromwich [10], the solution of (2.1) is given by

$$u(t) = \frac{1}{2\pi i} \int_{\Gamma} e^{zt} \hat{u}(z) dz, \tag{2.4}$$

where $\hat{u}(z) = (zI + A)^{-1}(u_0 + \hat{f}(z))$ and Γ is a straight line Bromwich contour which is parallel to the imaginary axis with all singularities of $\hat{u}(z)$ being located to the left of Γ. The straight line Bromwich contour integral (2.4), with $\Re(z) > 0$, is unstable for numerical integration since the multiplying factor e^{zt} is oscillatory on the Bromwich contour in case $\hat{u}(z)$ does not decay quickly enough as the imaginary part goes to $\pm\infty$. In order to avoid this problem it is suggested, for instance, as in [49], that the straight line Bromwich contour be deformed such that both head and tail lie in the left half plane so that the magnitude of e^{zt} decays quickly which enables highly oscillatory factors in the integrand to be negligible. Notice that the straight line contour Γ can be deformed as long as all singularities remain to the left of it.

Such a deformed contour can be parameterized by a suitable mapping $\phi : (a, b) \to \mathbb{C}$, with (a, b) being possibly an infinite interval, the formula (2.4) can be expressed as

$$u(t) = \frac{1}{2\pi i} \int_{a}^{b} e^{\phi(\omega)t} \hat{u}(\phi(\omega)) \phi'(\omega) d\omega. \tag{2.5}$$

By applying a suitable numerical quadrature to approximate the resulting integral in (2.5), one obtains a numerical inversion of Laplace transform.

In this chapter we first review and compare the most efficient methods for numerical Laplace inversion. And then we consider an roundoff error control, which extends the previous result (Weideman, 2010) to the case of numerical Laplace inversion for hyperbolic contour.

2.2 A unified framework to several numerical Laplace inversion schemes

There are three issues in the control of the numerical Laplace inversion: (i) the choice of contour Γ in (2.4), (ii) its parameterization ϕ to have the representation (2.5), and (iii) numerical quadrature in approximating the integral in (2.5).

In this section we examine and compare the three types of contours which have been recently popularized: parabolas [22, 23, 54], hyperbolas [21, 37, 40, 41, 42, 47, 54] and cotangent contours (Talbot's contour) [49, 53]. These contours being infinite, the natural choice of parameterization interval is $(-\infty, \infty)$. But for computational convenience, the infinite interval may be changed to a finite one. For instance, Sheen *et al.* [47] chose a hyperbola contour with parameter initially an infinite interval $(-\infty, \infty)$, which is then transformed to a finite interval $(-1, 1)$. Finally the integral over $(-1, 1)$ is approximated by the composite trapezoidal rule.

Here we discuss and examine several methods which have been studied, especially focusing on the three issues: the choice of contour shape, parameterization and quadrature.

2.2.1 Contours and their parameterization

Suppose that a deformed contour is represented in the following form:

$$\Gamma : z(\omega) = x(\omega) + iy(\omega) \quad \text{with } \omega \text{ runs from } -\infty \text{ to } +\infty \text{ such that } \lim_{\omega \to \pm\infty} x(\omega) = -\infty.$$

We consider the following three types of contours which have been used frequently in literature:

- the hyperbola-shape contours Γ_H [40, 41, 47, 54];

- the parabola-shape contours Γ_P [22, 23, 54];
- the cotangent-shape contours Γ_C [49, 53].

Let us describe the hyperbola and parabola types of contours first. In Cartesian coordinates, the general formula of a hyperbola which is symmetric with respect to the x-axis is given by

$$\frac{(x-x_0)^2}{a^2} - \frac{y^2}{b^2} = 1. \tag{2.6}$$

(H1) In [47] Sheen *et al.* proposed the hyperbola-type contour parameterized by

$$x(\omega) = \gamma - \sqrt{\omega^2 + \nu^2}, \quad y(\omega) = s\omega, \quad -\infty < \omega < \infty, \tag{2.7}$$

with suitable parameters $\gamma \in \mathbb{R}$ and $\nu, s > 0$. Here, $\gamma - \nu$ means its x-intercept and s the slope of the left branch of hyperbola.

(H2) Another type of hyperbolas introduced by M. López-Fernández & Palencia [40], M. López-Fernández *et al.* [41] and Weideman & Trefethen [54] can be parameterized as follows:

$$x(\omega) = \mu(1 - \sin\alpha\cosh\omega), \quad y(\omega) = \mu\cos\alpha\sinh\omega, \quad -\infty < \omega < \infty, \tag{2.8}$$

with suitable parameters $\mu, \alpha \in \mathbb{R}$.

Notice that both contours (2.7) and (2.8) can be interpreted as special forms of (2.6). The parameters (x_0, a, b) for (2.7) and (2.8) are given by $(\gamma, \nu, s\nu)$ and $(\mu, \mu\sin\alpha, \mu\cos\alpha)$, respectively.

Instead of (2.6), a hyperbola contour can be parameterized also in the form:

$$x(\omega) = x_0 - \sqrt{a^2 + (\frac{a}{b}\omega)^2}, \quad y(\omega) = \omega, \quad -\infty < \omega < \infty. \tag{2.9}$$

Turn to analyze parabola contours. The general form of a parabola which is symmetric with respect to the x-axis is

$$y^2 = 4p(x - x_0). \tag{2.10}$$

(P1) The parabola-type contours introduced by Gavrilyuk & Makarov [22, 23] are given by

$$x(\omega) = -a_0\omega^2 + b_0, \quad y(\omega) = \omega, \quad -\infty < \omega < \infty, \tag{2.11}$$

with suitable parameters $a_0, b_0 \in \mathbb{R}$.

(P2) Weideman & Trefethen [54] analyzed the parabola-type contours of the form

$$x(\omega) = \mu(1 - \omega^2), \quad y(\omega) = 2\mu\omega, \quad -\infty < \omega < \infty, \tag{2.12}$$

with suitable $\mu > 0$.

The parameters (x_0, p) for the contours (2.11) and (2.12) are given by $(b_0, -4a_0)$ and $(\mu, -\mu)$, respectively.

Parabola contours may be expressed as in the form:

$$x(\omega) = x_0 + \frac{1}{4p}\omega^2, \quad y(\omega) = \omega, \quad -\infty < \omega < \infty. \tag{2.13}$$

While the hyperbola and parabola types of contours have been proposed recently, the cotangent contour $\Gamma_C : z(\omega) = x(\omega) + iy(\omega)$ was introduced as

early as in 1979 by Talbot [49], and it was modified in [53] recently. With the parameters γ, μ and ν,

(C1) the Talbot contour [49] is given in the form

$$x(\theta) = \gamma + \mu \frac{\theta}{\tan\theta}, \quad y(\theta) = \mu\nu\theta, \quad -\pi < \theta < \pi; \tag{2.14}$$

(C2) the modified Talbot contour [53] is written in the form

$$x(\theta) = \gamma + \mu + \mu \frac{2\theta^2}{\theta^2 - \pi^2}, \quad y(\theta) = \mu\nu\theta, \quad -\pi < \theta < \pi. \tag{2.15}$$

Notice that (2.14) and (2.15) are parameterized by the variable θ in a finite range. However, one may attempt to represent them by a parameter in an infinite range as in (2.9). In the thread of these thoughts, one can write them in the form:

$$x(\omega) = \gamma + \mu\psi(\omega), \quad y(\omega) = \omega, \quad -\infty < \omega < \infty, \tag{2.16}$$

where $\psi(\omega) = \frac{\eta_1^{-1}(\frac{\omega}{\mu\nu})}{\tan(\eta_1^{-1}(\frac{\omega}{\mu\nu}))}$ for (2.14) and $\psi(\omega) = 1 + \frac{2[\eta_2^{-1}(\frac{\omega}{\mu\nu})]^2}{[\eta_2^{-1}(\frac{\omega}{\mu\nu})]^2 - \pi^2}$ for (2.15) with

$$\eta_1(\theta) := \begin{cases} 1 - \frac{\theta}{\tan\theta}, & -\pi < \theta < 0, \\ \frac{\theta}{\tan\theta} - 1, & 0 \le \theta < \pi, \end{cases} \quad \text{and} \quad \eta_2(\theta) := \begin{cases} -\frac{2\theta^2}{\theta^2 - \pi^2}, & -\pi < \theta < 0, \\ \frac{2\theta^2}{\theta^2 - \pi^2}, & 0 \le \theta < \pi. \end{cases} \tag{2.17}$$

By using the above contour representations (2.9), (2.13) and (2.16), the formula (2.4) takes the form

$$u(t) \;=\; \frac{1}{2\pi i} \int_{-\infty}^{\infty} e^{z(\omega)t} \hat{u}(z(\omega)) z'(\omega) d\omega, \tag{2.18}$$

where $\hat{u}(z(\omega)) = (zI + A)^{-1}(u_0 + \hat{f}(z(\omega)))$.

2.2.2 Infinity-to-finite interval maps and quadrature rule

In the preceding subsection the integral formula (2.4) is reduced to more tractable ones (2.18). The next procedure is to apply a change of variables that allows the parameter variable to be in a finite interval (for instance, see [15] also for such treatments). We want to change into the form:

$$u(t) = \int_{-1}^{1} g(y,t)dy.$$

The change of variables formula used in [47] is given by $\omega : (-1,1) \to (-\infty,\infty)$ defined by $\omega(y) = \frac{1}{\tau}\log\frac{1+y}{1-y}$ with the parameter $\tau > 0$. Hence one gets

$$\begin{aligned} u(t) &= \frac{1}{2\pi i}\int_{-\infty}^{\infty} e^{z(\omega)t}\hat{u}(z(\omega))z'(\omega)d\omega \\ &= \frac{1}{2\pi i}\int_{-1}^{1} e^{z(\omega(y))t}\ \hat{u}(z(\omega(y)))z'(\omega(y))\frac{d\omega}{dy}dy \\ &= \int_{-1}^{1} g(y,t)dy, \end{aligned} \tag{2.19}$$

where

$$g(y,t) = \frac{1}{2\pi i}e^{z(\omega(y))t}\ \hat{u}(z(\omega(y)))\ z'(\omega(y))\ \frac{d\omega}{dy}.$$

Let us consider the integral (2.19) and its trapezoidal approximation. We apply the composite trapezoidal rule based on an uniform subdivision of the interval [-1,1] with property that $g(y,t)$ vanishes at end points, which enables to apply Euler-Maclaurin type of fast convergence. The approximation of (2.19)

is given by

$$\begin{aligned} u_N(t) &= \sum_{j=-N+1}^{N-1} g(y_j,t)\Delta y \\ &= \sum_{j=-N+1}^{N-1} \frac{1}{2\pi i} e^{z(\omega(y_j))t} \hat{u}(z(\omega(y_j)))z'(\omega(y_j))\frac{d\omega}{dy}(y_j)\Delta y, \quad (2.20) \end{aligned}$$

where $y_j = j\Delta y,\ \Delta y = \frac{1}{N},\ j = -N+1, \cdots, N-1$. Here,

$$z(\omega(y)) = \gamma - \sqrt{\Big(\frac{1}{\tau}\log\frac{1+y}{1-y}\Big)^2 + \nu^2} + is\Big(\frac{1}{\tau}\log\frac{1+y}{1-y}\Big).$$

In López-Fernández *et al.* [41] the approximation of (2.18) by composite trapezoidal rule is given by

$$u_N(t) = h\sum_{j=-N}^{N} \frac{1}{2\pi i} e^{z(\omega_j)t}\hat{u}(z(\omega_j))z'(\omega_j), \quad (2.21)$$

where $\omega_j = jh$.

With a parameter h, the quadrature points used in Palencia *et al.* [40, 41] are as follows:

$$z(\omega) = \lambda\Big(1 - \sin\alpha\cosh\big(\sinh^{-1}(\frac{\omega}{\lambda\cos\alpha})\big)\Big) + i\omega.$$

Therefore if we introduce the finite interval-to-infinity map $\omega : [-1,1] \to (-\infty,\infty)$ defined by

$$\omega(y) = \lambda\cos\alpha\sinh(Nhy), \quad (2.22)$$

then one has

$$z(\omega(y)) = \lambda(1 - \sin\alpha\cosh(Nhy)) + i(\lambda\cos\alpha\sinh(Nhy)), \quad y \in [-1,1].$$

Notice that the range of the map ω defined by (2.22) is the truncated interval $[-\sinh(Nh), \sinh(Nh)]$ instead of the full infinity interval $(-\infty, \infty)$.

Turn to analyze the parabola-type contour. Recall that the contours [22, 54] considered its parameterization are respectively given by

$$z(\omega) = -a_0\omega^2 + b_0 + i\omega, \tag{2.23}$$

$$z(\omega) = \mu\Big(1 - \big(\frac{\omega}{2\mu}\big)^2\Big) + i\omega. \tag{2.24}$$

In I. P. Gavrilyuk and V. L. Makarov [22] the Sinc quadrature formula of (2.18) is given by

$$u_N(t) = \sum_{j=-N}^{N} \alpha_j e^{z_j t}\hat{u}(z_j), \tag{2.25}$$

with an appropriate parameter α_j used in [22] and the approximation by composite trapezoidal rule used the contour (2.24) in [54] is the same with (2.21).

Also, if we introduce the finite interval-to-infinity map $\omega : [-1, 1] \to (-\infty, \infty)$ defined by

$$\omega(y) = Nhy, \quad \text{or} \quad \omega(y) = 2\mu Nhy, \tag{2.26}$$

with the parameter h used in [22, 54] we obtain

$$z(\omega(y)) = -a_0(Nhy)^2 + b_0 + i(Nhy),$$

$$z(\omega(y)) = \mu(1 - (Nhy)^2) + i(2\mu Nhy),$$

respectively, for $y \in [-1, 1]$. As with the previous hyperbolic case, we note that the range of the map ω defined by (2.26) is the truncated interval $[-Nh, Nh]$

instead of the full infinity interval $(-\infty, \infty)$.

Finally, let us examine the Talbot contours used in [49, 53]. Its composite midpoint rule approximation of (2.18) is written by

$$u_N(t) = h \sum_{j=-N}^{N+1} \frac{1}{2\pi i} e^{z(\omega_j)t} \hat{u}(z(\omega_j)) z'(\omega), \tag{2.27}$$

where $\omega_j = (j + \frac{1}{2})h$. For the original Talbot contour [49] and the modified Talbot contour [53] we recall that the contour (2.16) represented by a variable in an infinite range:

$$z(\omega) = \gamma + \mu\psi(\omega) + i\omega,$$

where $\psi(\omega)$ is defined by (2.17).

Then, we are able to bring in the finite interval-to-infinity map $\omega_j : (-1, 1) \to (-\infty, \infty)$ respectively defined by

$$\omega_1(y) = \begin{cases} 1 - \frac{y\pi}{\tan(y\pi)}, & -1 < y < 0, \\ \frac{y\pi}{\tan(y\pi)} - 1, & 0 \le y < 1, \end{cases} \quad \text{and} \quad \omega_2(y) = \begin{cases} -\frac{2y^2}{y^2-1}, & -1 < y < 0, \\ \frac{2y^2}{y^2-1}, & 0 \le y < 1. \end{cases} \tag{2.28}$$

Then one gets, for $y \in (-1, 1)$,

$$z(\omega_1(y)) = \gamma + \mu\psi(\omega_1(y)) + i\omega_1(y),$$

for the original Talbot contour [49], and

$$z(\omega_2(y)) = \gamma + \mu\psi(\omega_2(y)) + i\omega_2(y),$$

for the modified Talbot contour [53].

Remark 2.2.1. Note that the range of the map ω defined by (2.28) is the full

infinity interval $(-\infty, \infty)$ while the range of the maps in (2.22) and (2.26) is not fully infinity interval, the truncated one.

So far, we have reviewed and compared several efficient methods for numerical Laplace inversion suggested in the original papers [22, 23, 40, 41, 47, 49, 53, 54]. Several methods have been classified and interpreted as the contents related to the following issues: (i) the choice of contour & its parameterization, and (ii) infinity-to-finite interval map & numerical quadrature rule. In short,

(i) Contour & parameterization

$$z(\omega) = x(\omega) + i\omega, \quad -\infty < \omega < \infty.$$

- Hyperbolic contour [40, 47, 54]: $z(\omega) = x_0 - \sqrt{a^2 + (\frac{a}{b}\omega)^2} + i\omega$,
- Parabolic contour [22, 23, 54]: $z(\omega) = x_0 + \frac{1}{4p}\omega^2 + i\omega$,
- Cotangent contour [49, 53]: $z(\omega) = \gamma + \mu\psi(\omega) + i\omega$.

(ii) Infinity-to-finite interval map & quadrature rule

- Sheen *et al.* (2003): $z(\omega(y)) = \gamma - \sqrt{\left(\frac{1}{\tau}\log\frac{1+y}{1-y}\right)^2 + \nu^2} + is\left(\frac{1}{\tau}\log\frac{1+y}{1-y}\right)$,
- López-Fernández & Palencia (2004):
  $z(\omega(y)) = \lambda(1 - \sin\alpha\cosh(Nhy)) + i(\lambda\cos\alpha\sinh(Nhy))$,
- Gavrilyuk & Makarov (2001): $z(\omega(y)) = -a_0(Nhy)^2 + b_0 + i(Nhy)$,
- Weideman & Trefethen (2007): $z(\omega(y)) = \mu(1 - (Nhy)^2) + i(2\mu Nhy)$,
- Talbot (1979): $z(\omega_1(y)) = \gamma + \mu\psi(\omega_1(y)) + i\omega_1(y)$,
- Weideman (2006): $z(\omega_2(y)) = \gamma + \mu\psi(\omega_2(y)) + i\omega_2(y)$,

for the parameter h used in original papers [22, 40, 54] and the quadrature point N.

2.3 Roundoff error control on numerical Laplace inversion

Using a suitable deformed contour, the formula (2.4) can be expressed as

$$u(t) = \frac{1}{2\pi i} \int_{-\infty}^{\infty} e^{z(\omega)t} \hat{u}(z(\omega)) z'(\omega) d\omega, \tag{2.29}$$

and applying a quadrature rule (here, we employ the midpoint rule) to the integral, it can be approximated by

$$u(t) \approx \frac{h}{2\pi i} \sum_{k=-N}^{N-1} e^{z(\omega_k)t} \hat{u}(z(\omega_k)) z'(\omega_k), \tag{2.30}$$

with $\omega_k = (k + 1/2)h$.

In numerical computations the effect of roundoff error should be considered to achieve accurate results. We remark that there are former researches to deal with the effect of roundoff error. In [36] Lee & Sheen discussed the roundoff error analysis for a deforming contour which consists of the union of circles. And for parabolic contour it was given in Weideman [52], hyperbolic contour in López-Fernández *et al.* [41].

In this section we extend the roundoff error model suggested by Weideman [52] to find the modified optimal parameter for hyperbolic contour which gives great efficiency. And an multi-precision arithmetic environment is considered to get more accurate results and compare the most efficient methods. First, we briefly describe the error analysis of Weideman & Trefethen [54]. And then the estimation of the roundoff error for hyperbola is derived. Finally several

numerical results are presented.

2.3.1 Review of error estimation

Before presenting the roundoff error control for numerical Laplace inversion, let us start with a review of error estimation in Weideman & Trefethen (2007) that is applied to find optimal parameters for parabola and hyperbola. They found the optimal parameters for the following scalar problem.

$$e^{\lambda t} = \frac{1}{2\pi i}\int_{\Gamma} \frac{e^{zt}}{z-\lambda} dz. \tag{2.31}$$

With a deformed contour used in [22, 23, 40, 41, 47, 52, 54] the formula (2.31) can be expressed as

$$e^{\lambda t} = \frac{1}{2\pi i}\int_{-\infty}^{\infty} \frac{e^{z(u)t}}{z(u)-\lambda} z'(u) du, \tag{2.32}$$

and applying the midpoint rule to the integral, it can be approximated by

$$e^{\lambda t} \approx \frac{h}{2\pi i}\sum_{k=-N}^{N-1} \frac{e^{z(u_k)t}}{z(u_k)-\lambda} z'(u_k), \tag{2.33}$$

with $u_k = (k+1/2)h$.

The error can be expressed as the sum of the discretization error and the truncation error as follows:

$$I - I_{h,N} = \underbrace{I - I_h}_{DE} + \underbrace{I_h - I_{h,N}}_{TE}. \tag{2.34}$$

Here,

$$I = \int_{-\infty}^{\infty} g(u)du, \quad I_h = h\sum_{k=-\infty}^{\infty} g(u_k), \quad \text{and} \quad I_{h,N} = h\sum_{k=-N}^{N-1} g(u_k),$$

where $g(u) = \frac{1}{2\pi i}\frac{e^{z(u)t}}{z(u)-\lambda}z'(u)$. Here the discretization error, DE is considered as the sum of two parts, DE_+ and DE_-. The DE_+ is related the distance to the pole λ from the contour and the DE_- implies the growth of the exponential factor e^{zt}.

Theorem 2.3.1 (Weideman & Trefethen [54]). *Let $w = u + iv$, with u and v real. Suppose $g(w)$ is analytic in the strip $-d < v < c$, for some $c > 0$, $d > 0$, with $g(w) \to 0$ uniformly as $|w| \to \infty$ in that strip. Suppose further that for some $M_+ > 0$, $M_- > 0$ the function $g(w)$ satisfies*

$$\int_{-\infty}^{\infty} |g(u + ir)|du \le M_+, \quad \int_{-\infty}^{\infty} |g(u - is)|du \le M_-,$$

for all $0 < r < c$, $0 < s < d$. Then

$$|I - I_h| \le DE_+ + DE_-,$$

where $DE_+ = \frac{M_+}{e^{2\pi c/h}-1}$, $\quad DE_- = \frac{M_-}{e^{2\pi d/h}-1}$.

Remark 2.3.2. *As already explained in [54], the discretization is given by*

$$DE_+ = \mathcal{O}\big(e^{-2\pi c/h}\big), \quad DE_- = \mathcal{O}\big(M_-(d)e^{-2\pi d/h}\big), \quad h \to 0,$$

for $c < \infty$, $d = \infty$. And the truncation error can be approximated by

$$TE = \mathcal{O}\big(|g(hN)|\big), \quad N \to \infty.$$

Using the above facts, the following error estimation can be obtained

$$DE_+ = \mathcal{O}\big(e^{-\frac{2\pi}{h}}\big), \quad DE_- = \mathcal{O}\big(e^{-\frac{\pi^2}{\mu t h^2}+\frac{2\pi}{h}}\big), \quad \text{and} \quad TE = \mathcal{O}\big(e^{\mu t(1-(hN)^2)}\big),$$

in the case of parabolic contour (2.12).

Balancing the above three error estimations, one gets

$$-\frac{2\pi}{h} = -\frac{\pi^2}{\mu t h^2} + \frac{2\pi}{h} = \mu t(1-(hN)^2), \qquad N \to \infty, \tag{2.35}$$

and then the optimal parameters can be obtained as follows

$$h_* = \frac{3}{N}, \quad \mu_* = \frac{\pi}{12}\frac{N}{t}. \tag{2.36}$$

Let us turn to the hyperbolic contour. The error estimation of hyperbolic contour (2.8) are given by

$$DE_+ = \mathcal{O}\big(e^{-\frac{2\pi(\pi/2-\alpha)}{h}}\big), \quad DE_- = \mathcal{O}\big(e^{\mu t - \frac{2\pi\alpha}{h}}\big), \quad \text{and} \quad TE = \mathcal{O}\big(e^{\mu t(1-\sin\alpha\cosh(hN))}\big).$$

Thus,

$$-\frac{2\pi(\frac{\pi}{2}-\alpha)}{h} = \mu t - \frac{2\pi\alpha}{h} = \mu t(1-\sin\alpha\cosh(hN)), \qquad N \to \infty. \tag{2.37}$$

From the above equalities, one can obtain the formula

$$hN = \cosh^{-1}\big(\frac{2\alpha}{(4\alpha-\pi)\sin\alpha}\big) := A(\alpha).$$

Hence, we can consider h and μ as function of α such that

$$h = \frac{A(\alpha)}{N}, \quad \mu = \frac{4\pi\alpha - \pi^2}{A(\alpha)}\frac{N}{t}. \tag{2.38}$$

Assume that $\alpha \in (\pi/4, \pi/2)$. Then, the error convergence rate of DE_+ is $\mathcal{O}\big(e^{-\frac{\pi^2-2\pi\alpha}{A(\alpha)}N}\big)$, and $-\frac{\pi^2-2\pi\alpha}{A(\alpha)}$ has a maximum at $\alpha_* = 1.1721$. Finally, the optimal parameters of α, h, μ can be calculated

$$\alpha_* = 1.1721, \quad h_* = \frac{1.0818}{N}, \quad \mu_* = 4.4921\frac{N}{t}. \tag{2.39}$$

As already mentioned in [52], the effects of roundoff errors should be considered when these optimal parameters (2.36), (2.39) are used to compute the numerical integration (2.33). We examine those in the next subsection.

2.3.2 Roundoff error control for hyperbolic contour

In this subsection, we briefly give an overview of the method of roundoff error control for parabolic contour (see [52] for details) and then develop the result for the hyperbolic contour.

Consider

$$I_{h,N,\epsilon} = h \sum_{k=-N}^{N-1} g(u_k)(1+\epsilon_k), \tag{2.40}$$

where ϵ_k is the relative error, it is satisfied $|\epsilon_k| \leq \epsilon$, for machine precision epsilon ϵ.

Then, the total error (2.34) can be extended to

$$I - I_{h,N,\epsilon} = \underbrace{I - I_h}_{DE} + \underbrace{I_h - I_{h,N}}_{TE} + \underbrace{I_{h,N} - I_{h,N,\epsilon}}_{RE}, \tag{2.41}$$

where $\mathrm{RE} = h\sum_{k=-N}^{N-1} g(u_k)\epsilon_k$. For the scalar problem, one can get the following inequality.

$$|RE| \leq \epsilon \frac{1}{\pi} \max_k |e^{z(u_k)t}| h \sum_{k=0}^{N-1} \Big| \frac{z'(u_k)}{z(u_k) - \lambda} \Big|. \tag{2.42}$$

For the parabolic contour used in [52], the roundoff error can be estimated as

$$|RE| \approx \epsilon e^{\mu t} = e^{\log \epsilon + \mu t}, \tag{2.43}$$

and then the error equation (2.35) is extended to

$$-\frac{2\pi}{h} = -\frac{\pi^2}{\mu t h^2} + \frac{2\pi}{h} = \mu t(1-(hN)^2) = \log\epsilon + \mu t. \tag{2.44}$$

From the above equation (2.44), the modified optimal parameters are explicitly given by

$$\mu_* = \frac{\log^3\left(\frac{1}{\epsilon}\right)}{4t\pi^2 N^2}, \quad h_* = \frac{2\pi}{\log\left(\frac{1}{\epsilon}\right)} + \frac{\log\left(\frac{1}{\epsilon}\right)}{2\pi N^2}, \tag{2.45}$$

provided machine precision epsilon and N are fixed.

From our examples in Subsection 2.4, we can conclude that the method which hyperbola is used as contour is more efficient than the case of using parabola. But it may be thought of poor results without considering the roundoff error. From now, we give the roundoff error analysis for hyperbolic contour.

Let us consider the following hyperbolic contour used in [54].

$$z(u) = \mu(1+\sin(iu-\alpha)). \tag{2.46}$$

With this contour the followings hold.

(i) $\max_k |e^{z(u_k)t}| \le e^{\mu(1-\sin\alpha)t}$, for $\alpha \in (\frac{\pi}{4}, \frac{\pi}{2})$.

(ii) $h\sum_{k=0}^{N-1}\left|\frac{z'(u_k)}{z(u_k)-\lambda}\right|$ is bounded as $N\to\infty$.

From (i),(ii) we estimate the roundoff error as follows.

$$|RE| \approx \epsilon\ e^{\mu(1-\sin\alpha)t} = e^{log\epsilon+\mu(1-\sin\alpha)t}, \tag{2.47}$$

with a machine precision epsilon $\epsilon = 10^{-16}$.

Thus, the error equation for hyperbola (2.37) can be extended to

$$-\frac{2\pi(\frac{\pi}{2}-\alpha)}{h} = \mu t - \frac{2\pi\alpha}{h} = \mu t(1-\sin\alpha\cosh(hN)) = \log\epsilon + \mu t(1-\sin\alpha). \tag{2.48}$$

Rearranging the last equality of (2.48), one knows

$$\cosh(hN) = \frac{h\ \log\left(\frac{1}{\epsilon}\right)}{(4\pi\alpha-\pi^2)\sin\alpha} + 1.$$

And using the same notation with (2.38), we get the following:

$$\begin{aligned} N &= \frac{A(\alpha)}{\cosh A(\alpha)-1}\frac{\log\left(\frac{1}{\epsilon}\right)}{(4\pi\alpha-\pi^2)\sin\alpha} \\ &= \frac{A(\alpha)\log\left(\frac{1}{\epsilon}\right)}{\pi\{2\alpha-(4\alpha-\pi)\sin\alpha\}}. \end{aligned} \tag{2.49}$$

With the original optimal parameter $\alpha_* = 1.1721$ in [54], we approximate the value of quadrature point N,

$$N_* \approx 13.809.$$

In Figure 2.1(a), the error starts to increase when N is greater than N_*. It is well-known result due to roundoff errors. To avoid this problem, the new optimal parameter for hyperbolic contour (2.46) should be determined.

For $\alpha_* = 1.1721$, one can easily know that the roundoff error, $RE \approx e^{\log\epsilon+0.3523N}$, dominates the $DE_- \approx e^{-2.3156N}$ for large N. Thus, the following equation is sufficient to deal with the roundoff error.

$$-\frac{2\pi(\frac{\pi}{2}-\alpha)}{h} = \mu t(1-\sin\alpha\cosh(hN)) = \log\epsilon + \mu t(1-\sin\alpha). \tag{2.50}$$

From now on, we want to find optimal parameters h and μ which can help to

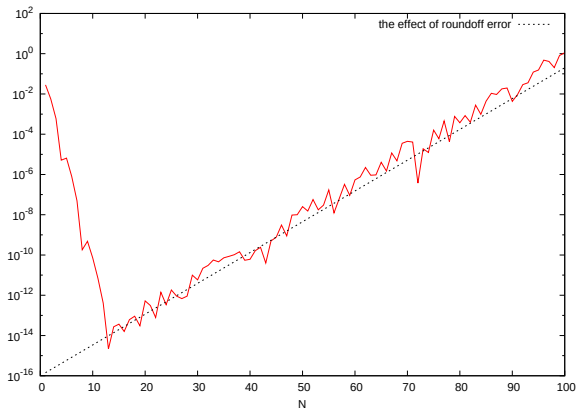

(a)

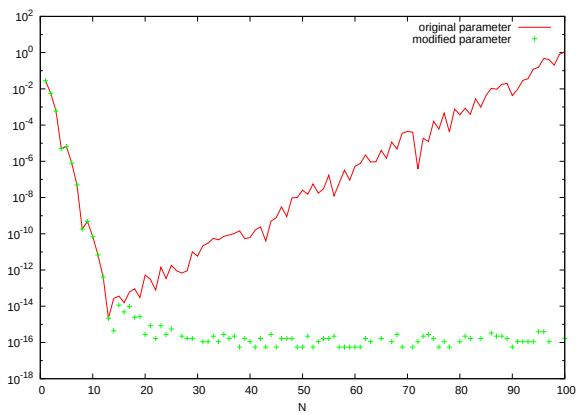

(b)

Figure 2.1 Error curve in double-precision environment in approximating e^{-t} at $t = 1$ using the hyperbolic contour (2.46) with the original optimal parameters in (2.39) (left), with the original optimal parameters in (2.39) for $N \leq 13$ and the modified optimal parameters in (2.55) for $N \geq 14$ (right). Here the dash-line in left figure represents the effect of roundoff errors, $\epsilon e^{\mu(1-\sin\alpha)t} = \epsilon e^{0.3523N}$ in (2.47).

reduce the roundoff error on numerical Laplace inversion.

This can be rewritten as follows:

$$\begin{cases} -\dfrac{2\pi(\frac{\pi}{2}-\alpha)}{h} = \mu t(1-\sin\alpha\cosh(hN)), \\ -\dfrac{2\pi(\frac{\pi}{2}-\alpha)}{h} = \log\epsilon + \mu t(1-\sin\alpha). \end{cases} \tag{2.51}$$

From the second equation of (2.51), one gets

$$\mu t = -\frac{1}{1-\sin\alpha}\Big(\frac{2\pi(\frac{\pi}{2}-\alpha)}{h} + \log\epsilon\Big). \tag{2.52}$$

Inserting (2.52) into the first equation of (2.51), we can obtain

$$\frac{\sin\alpha}{1-\sin\alpha}\Big(\frac{2\pi(\frac{\pi}{2}-\alpha)}{h}+\log\epsilon\Big)\cosh(hN)+(1-\frac{1}{1-\sin\alpha})\frac{2\pi(\frac{\pi}{2}-\alpha)}{h}-\frac{\log\epsilon}{1-\sin\alpha}=0.$$

Finally, one can write

$$\cosh(hN) = 1 + \frac{(1-\sin\alpha)\log\epsilon}{\Big(\frac{2\pi(\frac{\pi}{2}-\alpha)}{h}+\log\epsilon\Big)\sin\alpha}.$$

Let $hN := R$. Then,

$$h_* = \frac{R}{N}, \qquad \mu_* = \frac{\log\epsilon}{t(1-\cosh R)\sin\alpha}, \tag{2.53}$$

satisfying

$$\cosh R = 1 + \frac{(1-\sin\alpha)\log\epsilon}{\Big(2\pi(\frac{\pi}{2}-\alpha)\frac{N}{R}+\log\epsilon\Big)\sin\alpha}. \tag{2.54}$$

Now, let us find solution R of the equation (2.54). To simplify the above equation, we assume that $\cosh R$ can be approximated to $1 + cR^2$, with a

suitable constant c.

$$\begin{aligned} \Longrightarrow \quad & cR^2 = \frac{(1-\sin\alpha)\log\epsilon}{\Big(2\pi(\frac{\pi}{2}-\alpha)\frac{N}{R}+\log\epsilon\Big)\sin\alpha}, \\ \Longrightarrow \quad & R^2 + \Big(\frac{\pi(\pi-2\alpha)}{\log\epsilon}N\Big)R - \frac{(1-\sin\alpha)}{c\sin\alpha} = 0. \end{aligned}$$

That is,

$$\begin{aligned} R &= \frac{1}{2}\Big(-\frac{\pi(\pi-2\alpha)}{\log\epsilon}N + \sqrt{\big(\frac{\pi(\pi-2\alpha)}{\log\epsilon}N\big)^2 + 4\frac{(1-\sin\alpha)}{c\sin\alpha}}\Big) \\ &\approx \frac{\pi(\pi-2\alpha)N}{\log\big(\frac{1}{\epsilon}\big)} + \frac{(1-\sin\alpha)}{c\sin\alpha}\frac{\log\big(\frac{1}{\epsilon}\big)}{\pi(\pi-2\alpha)N}. \end{aligned}$$

Hence, the modified optimal parameters h_*, μ_* are given by, for large N,

$$\begin{cases} h_* = \dfrac{\pi(\pi-2\alpha)}{\log\big(\frac{1}{\epsilon}\big)} + \dfrac{(1-\sin\alpha)\log\big(\frac{1}{\epsilon}\big)}{c\pi(\pi-2\alpha)\sin\alpha}\dfrac{1}{N^2}, \\ \mu_* = \dfrac{\log\big(\frac{1}{\epsilon}\big)}{t\Big(\cosh\big(\frac{\pi(\pi-2\alpha)}{\log\big(\frac{1}{\epsilon}\big)}N + \frac{(1-\sin\alpha)\log\big(\frac{1}{\epsilon}\big)}{c\pi(\pi-2\alpha)\sin\alpha}\frac{1}{N}\big) - 1\Big)\sin\alpha}, \end{cases} \tag{2.55}$$

where $\alpha = \alpha_* = 1.1721$, and a suitable constant c. Hence, modified optimal parameters can be obtained.

$$h_* = -\frac{2.5051}{\log\epsilon} - 0.0571\frac{\log\epsilon}{N^2}, \quad \mu_* = \frac{1.0851\ \log\epsilon}{\Big(1-\cosh\big(\frac{2.5051}{\log\epsilon}N + 0.0571\frac{\log\epsilon}{N}\big)\Big)t}. \tag{2.56}$$

Remark 2.3.3. *Since we know* $R \approx 1$ *from* (2.39)*, we can assume that* $\cosh R$ *can be approximated to* $1 + cR^2$*, and choose* c *as* 0.5946.

Type	Machine precision (ϵ)	Estimated N (N_*)
Single	10^{-7}	6.041
Double	10^{-16}	13.809
Multi	10^{-39}	33.659
Multi	10^{-58}	50.059

Table 2.1 Test environment

With these new parameters in (2.56), we found that the effect of roundoff error can be removed when N is large. (See Figure 2.1(b).)

So far, all computations are limited to an double-precision environment. Here we apply several arbitrary-precision arithmetic environment to check our modified optimal parameters in (2.55) work well. Two basic format (single, double) and two high-precisions are considered. With (2.49) the values of N_* which involve roundoff errors can be calculated on each of precisions (Table 2.1). To adopt multi-precision calculation we use Fujiwara's EXFLIB [19, 20]. All results are shown that error curves do not increase when N is large and remain at machine precision epsilon level when N is larger than N_*.

2.4 Numerical examples

In this section, we give some numerical examples. To avoid the effect of roundoff error all computations were implemented in multi-precision arithmetic environment and to compare the most efficient methods we consider several methods which are based on different contours: parabola [22, 23, 54] , hyperbola [40, 41, 42, 47, 54] , and cotangent contour [49, 53]. Here we compute discrete L^2-errors for $0 \le t \le 10$, *i.e.,*

$$E = \sqrt{\sum_{j=1}^{100} \big(u(t_j) - u_N(t_j)\big)^2/10}, \quad \text{where} \quad t_j = j/10,\ j = 0, 1, \cdots, 100$$

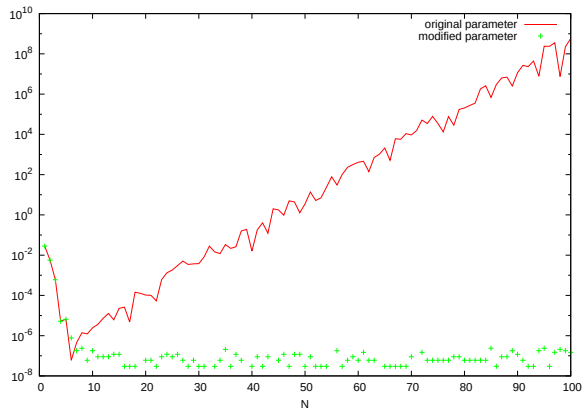

(a) Single-precision(=7) environment

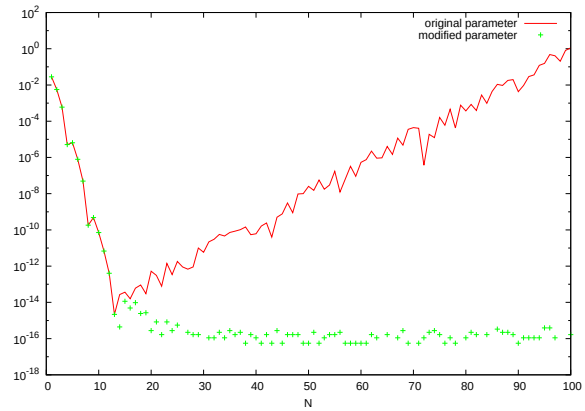

(b) Double-precision(=16) environment

Figure 2.2 Error curve in different-precision environment in approximating e^{-t} at $t = 1$ using the hyperbolic contour (2.46) with the original optimal parameters in (2.39) for $N \leq N_*$ and the modified optimal parameters in (2.55) for $N > N_*$.

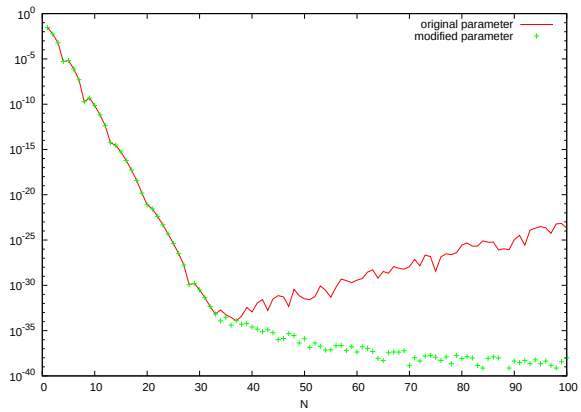

(a) Multi-precision(=39) environment

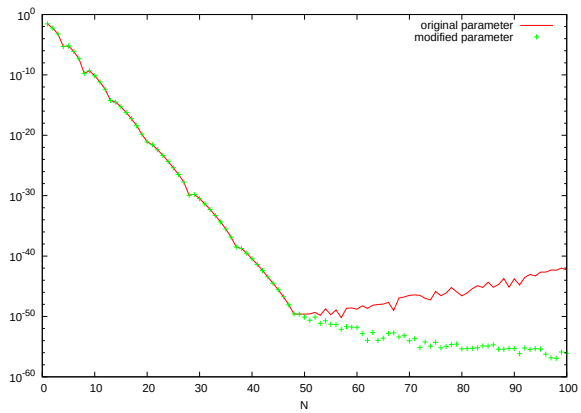

(b) Multi-precision(=58) environment

Figure 2.3 Error curve in different-precision environment in approximating e^{-t} at $t = 1$ using the hyperbolic contour (2.46) with the original optimal parameters in (2.39) for $N \leq N_*$ and the modified optimal parameters in (2.55) for $N > N_*$.

Example 2.4.1 (Exponential function)**.** We start to consider a simple differential equation. In case of A=I, f(t)=0 for (2.1). i.e.,

$$u_t + u = 0, \quad \text{for} \quad t > 0, \quad \text{with } u(0) = 1,$$

whose solution and its Laplace transform are given by $u(t) = e^{-t}$ and $\hat{u}(z) = (z+1)^{-1}$, respectively. Since the only singularity of $\hat{u}(z) = (z+1)^{-1}$ is -1, one can easily apply several contours and obtain the original function without any difficulties. However, one can observe that the error starts to grow as N gets larger in Table 2.2, which is due to the roundoff error. In order to resolve this problem, we adopted a multi-precision calculation using Fujiwara's EXFLIB [19, 20]. Improved results are shown in Table 2.3.

Example 2.4.2 (Several test functions)**.** Next, we tested several functions in Table 2.4, taken from Davies and Martin [14]. In the Laplace inversion we used the modified Talbot‘s contour [53], the parabola contour [54], and the hyperbola contour [47, 54]. The parameters used in our calculation are taken from [53, 54]. Numerical results in multi-precision using again Fujiwara's EXFLIB are shown in Table 2.5, Figures 2.4 – 2.8. We observe from Table 2.5 that the hyperbola is more efficient than both the parabola and Talbot's contour at least when we used the parameters suggested in [53, 54].

N	Hyperbola	Parabola	Talbot's
10	9.081E-11	7.855E-10	1.994E-07
20	8.613E-13	7.028E-15	3.150E-14
40	7.314E-10	2.945E-12	4.192E-12
80	2.351E-03	1.422E-07	1.460E-07

Table 2.2 Example 2.4.1: L^2-Errors in double-precision in approximating an exponential function

N	Hyperbola	Parabola	Talbot's
10	9.076E-11	7.853E-10	1.992E-07
20	7.283E-21	6.291E-19	3.424E-14
40	4.742E-41	3.365E-37	1.531E-27
80	3.619E-81	1.515E-73	2.922E-53

Table 2.3 Example 2.4.1: L^2-Errors in multi-precision(=100) in approximating an exponential function

$u_1(t) = 1$	$\hat{u}_1(z) = z^{-1}$
$u_2(t) = t$	$\hat{u}_2(z) = z^{-2}$
$u_3(t) = \sin t$	$\hat{u}_3(z) = (z^2+1)^{-1}$
$u_4(t) = t\cos t$	$\hat{u}_4(z) = (z^2-1)(z^2+1)^{-2}$
$u_5(t) = te^{-t}$	$\hat{u}_5(z) = (z+1)^{-1}$
$u_6(t) = e^{-t/2}$	$\hat{u}_6(z) = (z+1/2)^{-1}$
$u_7(t) = e^{-0.2t}\sin t$	$\hat{u}_7(z) = ((z+0.2)^2+1)^{-1}$
$u_8(t) = 2e^{-4/t}(\pi t^3)^{-1/2}$	$\hat{u}_8(z) = e^{-4z^{1/2}}$
$u_9(t) = (\pi t)^{-1/2}\cos(2t^{1/2})$	$\hat{u}_9(z) = z^{-1/2}e^{-z^{-1}}$
$u_{10}(t) = (e^{-t/4} - e^{-t/2})(4\pi t^3)^{-1/2}$	$\hat{u}_{10}(z) = (z+1/2)^{1/2} - (z+1/4)^{1/2}$

Table 2.4 Example 2.4.2: List of test functions used in the example

Test function	Hyperbola		Parabola		Talbot's	
	N=40	N=80	N=40	N=80	N=40	N=80
u_1	3.767E-40	2.166E-80	2.659E-36	1.093E-72	1.710E-27	2.872E-53
u_2	6.473E-37	7.661E-77	5.038E-33	4.162E-69	2.109E-28	6.147E-55
u_3	9.654E-18	3.139E-48	1.748E-12	7.106E-39	3.954E-10	1.014E-38
u_4	3.177E-16	1.030E-46	7.603E-11	8.500E-37	1.401E-08	7.164E-37
u_5	5.315E-40	4.006E-80	3.947E-36	2.277E-72	2.086E-28	5.249E-55
u_6	7.994E-41	4.457E-81	5.749E-37	2.167E-73	1.619E-27	2.898E-53
u_7	6.238E-21	2.461E-52	9.772E-16	8.537E-43	6.671E-13	3.681E-42
u_8	1.369E-46	8.429E-88	1.032E-41	7.817E-79	1.200E-29	9.659E-59
u_9	3.589E-35	1.890E-73	6.251E-31	1.209E-65	5.131E-27	3.900E-52
u_{10}	1.070E-41	6.399E-82	6.843E-38	2.740E-74	5.903E-28	4.882E-53

Table 2.5 Example 2.4.2: L^2-Errors in multi-precision(=100) environment in approximating several test functions in Table 2.4

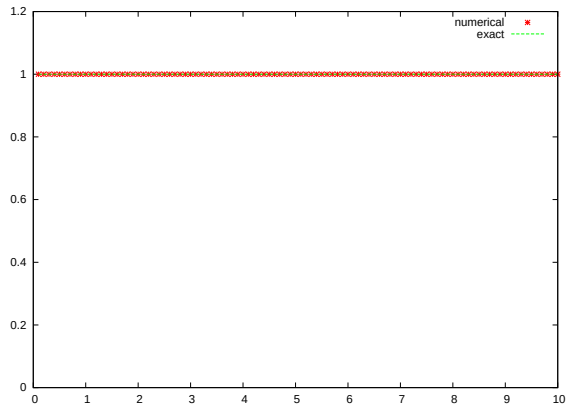

(a) $u_1(t)$

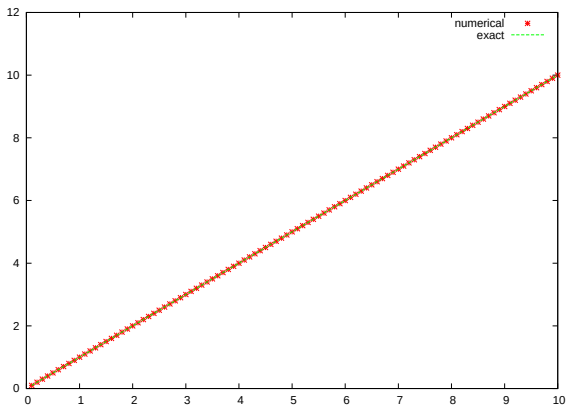

(b) $u_2(t)$

Figure 2.4 Example 2.4.2: Approximation of several test functions listed in Table 2.4 in double precision

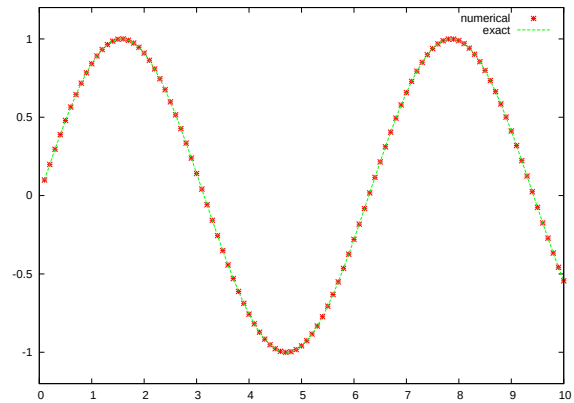

(a) $u_3(t)$

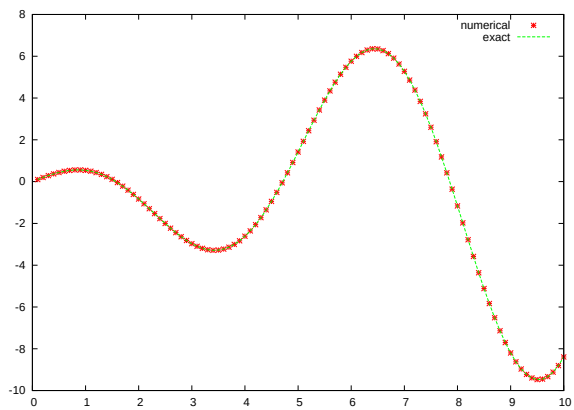

(b) $u_4(t)$

Figure 2.5 Example 2.4.2: Approximation of several test functions listed in Table 2.4 in double precision

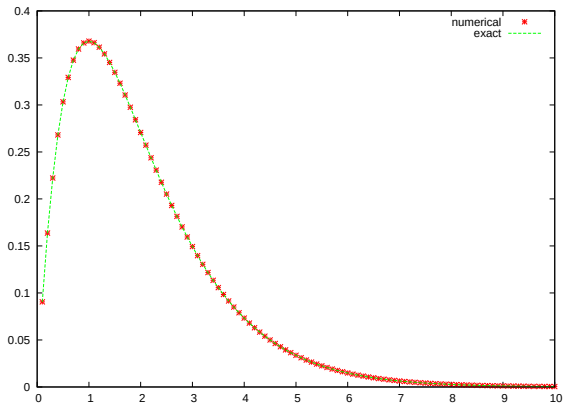

(a) $u_5(t)$

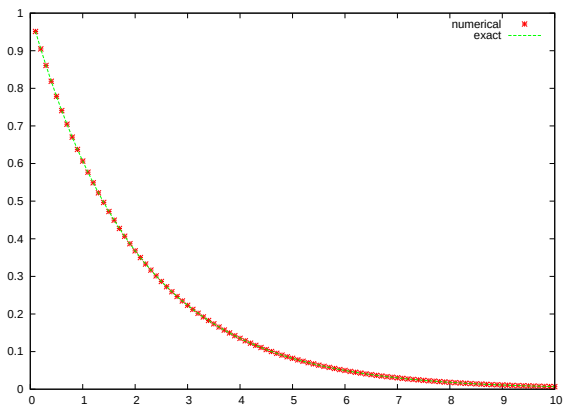

(b) $u_6(t)$

Figure 2.6 Example 2.4.2: Approximation of several test functions listed in Table 2.4 in double precision

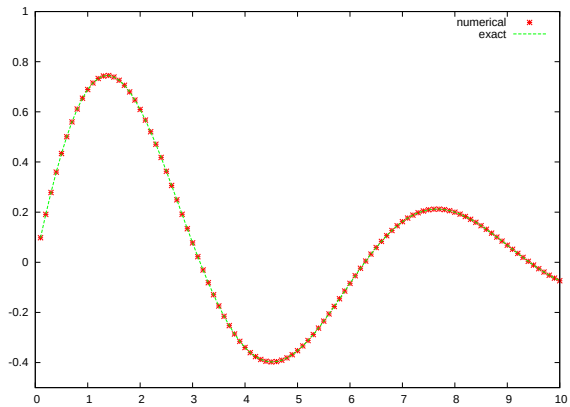

(a) $u_7(t)$

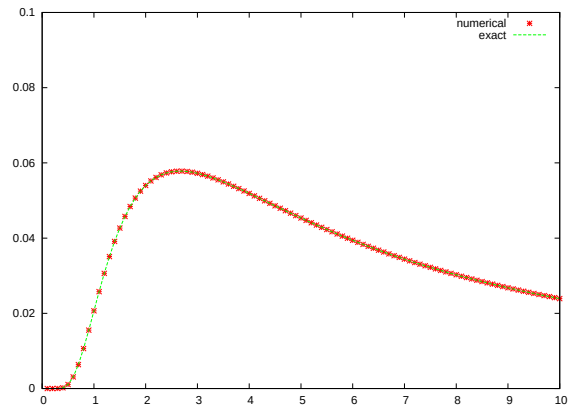

(b) $u_8(t)$

Figure 2.7 Example 2.4.2: Approximation of several test functions listed in Table 2.4 in double precision

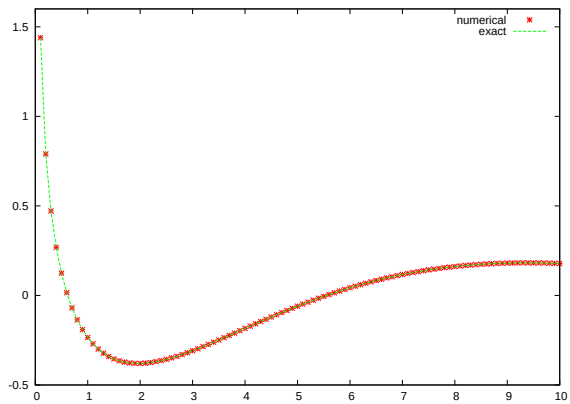

(a) $u_9(t)$

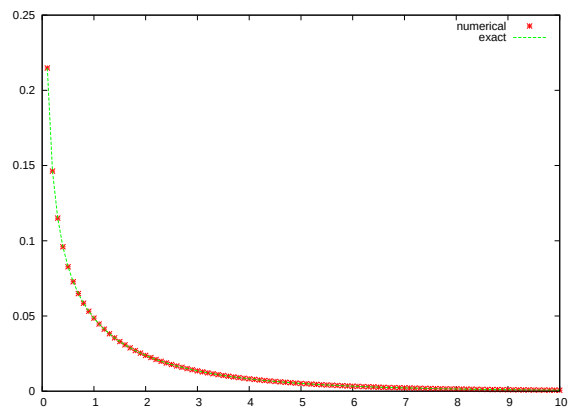

(b) $u_{10}(t)$

Figure 2.8 Example 2.4.2: Approximation of several test functions listed in Table 2.4 in double precision

Example 2.4.3 (Bessel function $J_0(t)$)**.** We consider the Bessel's differential equation

$$t^2 y'' + ty' + t^2 y = 0, \tag{2.57}$$

for which the Bessel function $J_0(t)$ of the first kind of order zero is one of the solutions. The Laplace transform of $J_0(t)$ is given by $\hat{u}(z) = \frac{1}{\sqrt{z^2+1}}$.

In case the branch cut of $\sqrt{z^2+1}$ is not treated carefully, the numerical Laplace inversion with a hyperbola contour would lead to the solution shown in Figure 2.9(a). which certainly deviates from the original Bessel function $J_0(t)$, especially at the numerical approximation would not reproduce the exact value one at $t = 0$.

This deviation is because of the choice of wrong branch cut adopted in the standard environment in programming languages, where the branch cut of square root function is given along the negative axis. To fix the choice of wrong branch cut problem, we defined the Laplace transform $\hat{u}(z)$ of the Bessel

N	Hyperbola	Parabola	Talbot's
10	0.391	0.453	0.668
20	1.588E-05	2.016E-02	0.261
40	8.324E-10	3.631E-12	2.611E-11
80	2.665E-03	1.684E-07	1.755E-07

Table 2.6 Example 2.4.3: L^2-Errors in double-precision in approximating the bessel function in the choice of right branch cut

N	Hyperbola	Parabola	Talbot's
10	0.391	0.453	0.668
20	1.588E-05	2.016E-02	0.261
40	7.658E-19	1.689E-13	2.470E-11
80	3.643E-49	2.319E-39	5.858E-40

Table 2.7 Example 2.4.3: L^2-Errors in multi-precision in approximating the bessel function in the choice of right branch cut

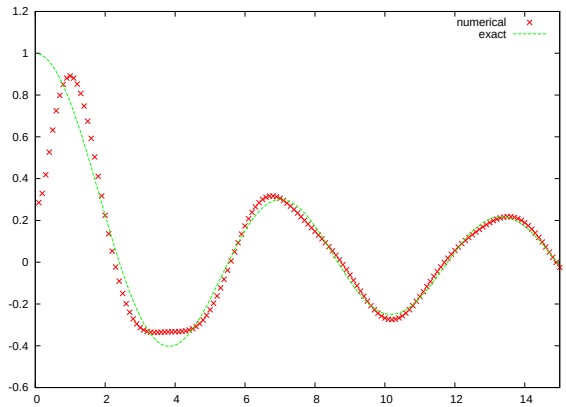

(a) the choice of wrong branch cut

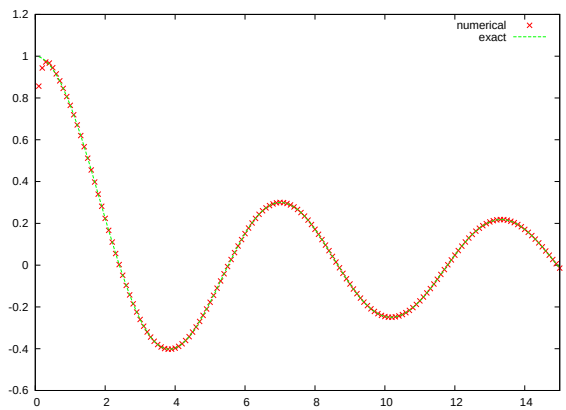

(b) the choice of right branch cut

Figure 2.9 Example 2.4.3: The significance in the choice of branch cut in approximating $J_0(t)$: in both figures the points and lines represent the exact and numerical solutions in double precision, respectively.

function in the following form;

$$\hat{u}(z) := \begin{cases} \frac{1}{\sqrt{z^2+1}} & \Re z > 0, \\ -\frac{1}{\sqrt{z^2+1}} & \Re z < 0. \end{cases}$$

Then applying the numerical inverse Laplace transform using a hyperbola, we could recover the original bessel function J_0 very successfully. The numerical results, still in double precision, are shown in Figure 2.9(b).

At a certain large time t, the numerical solution starts to be oscillatory and unstable, which is due to the roundoff error as shown in Figure 2.10(a). We again calculated using the Fujiwara's EXFLIB multi-precision package. The numerical result shown in Figure 2.10(b) is quite satisfactory at least up to $t = 100$.

Example 2.4.4 (Square wave)**.** So far we have examined only continuous functions. We now explore the case of discontinuous functions. We look at one of the typical discontinuous functions, namely, the square wave, whose Laplace transform, $\hat{u}(z) = 1/(z(1 + e^{-z}))$, has an infinite number of poles $(0, \pm\pi i, \pm 2\pi i, \cdots)$ on the imaginary axis. When we apply several approaches in double precision in obtaining its inverse Laplace transform, roundoff errors are dominating factors to produce unacceptable solutions as shown in Table 2.8. In order to cure this problem, the calculations in multi-precision showed significant progress compared to those in double-precision. However, even though we employ multi-precision (=100) environment, numerical solutions begin to converge to the target function as a sufficiently large number of quadrature points N are chosen (see Table 2.9 and Figure 2.12). This improvement comes from the fact that the larger N is chosen, the more singularities of its Laplace transform are contained in the left side of the contour which

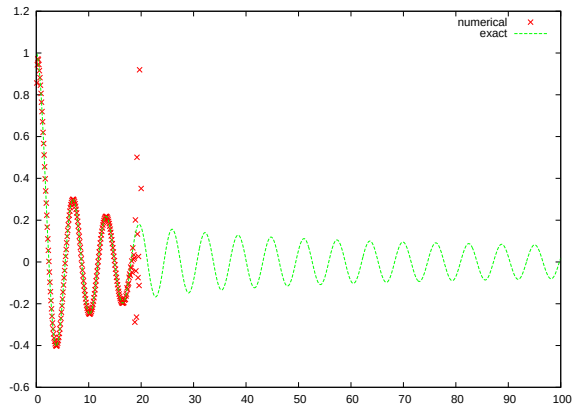

(a) double-precision

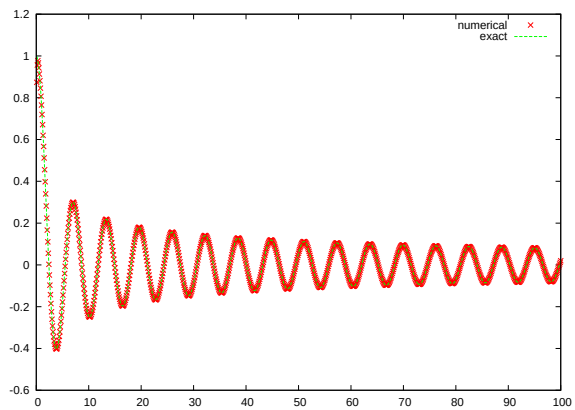

(b) multi-precision(=100)

Figure 2.10 Example 2.4.3: The consequence of roundoff error in approximating $J_0(t)$: the left figure calculated in double precision starts to deviate around $t = 20$ while that in multiple precision stays in good agreement at least until $t = 100$.

we are considering. This produce more accurate calculation. However roundoff errors increase as the number of quadrature points N increases, as shown in the case of $N = 1280$. But this problem may be alleviated by using higher precision.

N	Hyperbola	Parabola	Talbot's
10	1.393	1.386	NaN
20	1.122	1.273	NaN
40	NaN	NaN	NaN

Table 2.8 Example 2.4.4: L^2-Errors in double-precision in approximating a square wave

N	Hyperbola	Parabola	Talbot's
10	1.384	1.377	1.423
20	1.111	1.263	1.474
40	0.543	0.925	1.034
80	0.338	0.397	0.421
160	0.159	0.247	0.306
320	0.102	0.111	0.140
640	4.458E-02	6.886E-02	9.472E-02
1280	5.034E+81	1.127E+30	8.664E+23

Table 2.9 Example 2.4.4: L^2-Errors in multi-precision(=100) in approximating a square wave

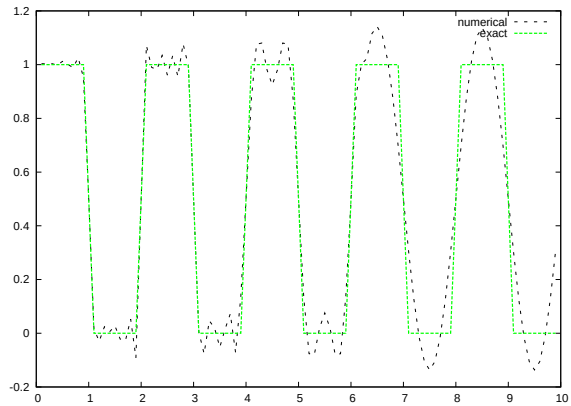

(a) N=80

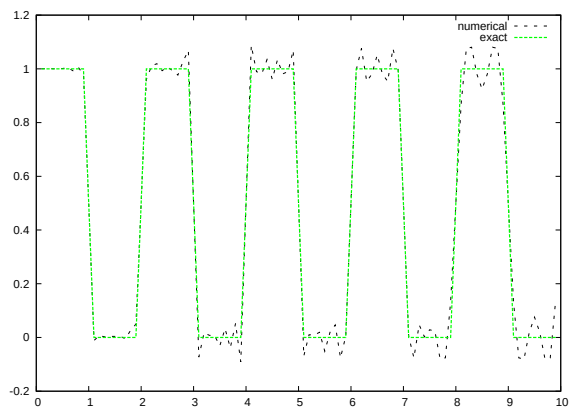

(b) N=160

Figure 2.11 Example 2.4.4: The approximation in multiple precision of a square wave with increasing number of quadrature points

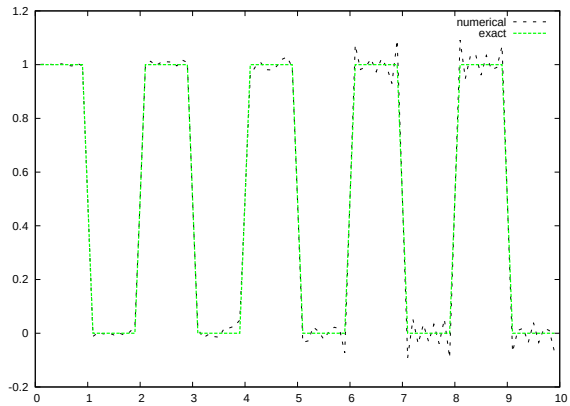

(a) N=320

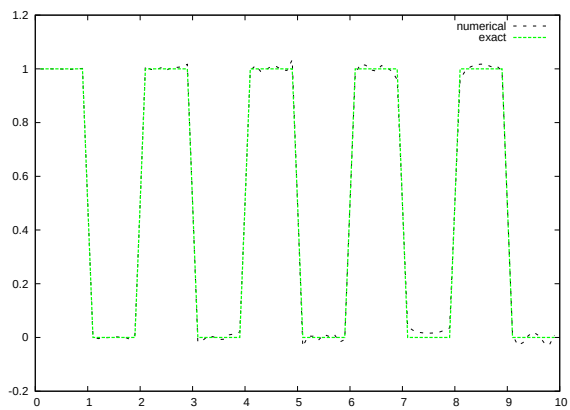

(b) N=640

Figure 2.12 Example 2.4.4: The approximation in multiple precision of a square wave with increasing number of quadrature points

Chapter 3

Weather Derivatives

3.1 Introduction

On January 4, 2010 there was a 25.8 centimeters snowfall in the central area of Korea encompassing the Capital Region and Gangwon-do, a record-breaking event since 1937. This heavy snowfall temporarily paralyzed transportation in that large area, and caused numerous accidents on the icy roads. Many agricultural facilities, including the ginseng greenhouses, were also broken by the weight of the piled-up snow. The loss of property caused by this snowfall was estimated to total 10.6 billion won. Apart from heavy snowfalls, the extreme weather events in Korea include unexpectedly intensive typhoons, heavy rains and heat waves in summer, and very cold winters. The cost of the annual average weather damage during the last ten years has been estimated to be more than 2 trillion won, so financial losses due to weather risks should be covered by adequate weather-related insurances and derivatives. However, the Korean insurance market is rather stagnant, especially in regard to weather

risks. According to the General Insurance Association of Korea, the number of weather-related contracts was thirty-six in 2002, twenty-seven in 2003, and forty-one in 2004. Although the market may be growing, it is restricted to contingency insurance where the insurance companies compensate the insured for damages that actually happen, and the proper estimation of total losses between the policyholders and the companies remains highly controversial.

The importance of weather risk has been recognized in most developed countries, where it is fast becoming customary to provide against uncertain climatic change. The typical provision includes the introduction of weather derivatives and associated Risk Management. An early weather transaction was executed by Aquila Energy, which structured a dual-commodity hedge for the Edison Company in 1996. Over-the-counter (OTC) weather derivatives have been traded since 1997, and at the Chicago Mercantile Exchange (CME) since the summer of 1999. In September 2003, the CME launched seasonality products for ten new cities, and then monthly for a list of twelve cities in the USA that was expanded to include five European cities. The CME now offers temperature products for twenty-four cities in the USA, six in Canada, eleven in Europe, three in Australia, and three elsewhere in the Asia-Pacific — cf. Tables 3.1 and 3.2). In addition to the increasing number of cities covered at the CME, the volume of weather derivative contracts issued has significantly increased — from 630,000 in 2005 to 798,000 in 2006, and to nearly 1,000,000 in 2007 [13, 43]. Although the volume did fall by about 16 % in 2008, that occurred during the onset of the current global financial crisis.

With the rapid growth of weather-related industries, relevant futures prices have been studied extensively [2, 3, 4, 5, 6, 9, 12, 16, 25, 34, 38, 24, 26, 29, 39, 46, 48, 50, 51, 55]. Since weather derivatives are non-tradable, no-arbitrage models (such as the Black-Scholes model) are inapplicable to pricing weather

options, directly. In 2000, Dornier & Querel [16] used mean-reverting Itô diffusions based on a standard Brownian motion to model Chicago temperature data. Brody *et al.* [9] proposed another dynamical model based on a fractional Brownian motion, and Alaton *et al.* [2] applied the Ornstein-Uhlenbeck process with a monthly variation to analyze the temperature at the Bromma Airport, Stockholm. Benth *et al.* [4, 5] generalized Dornier & Querel's approach by employing continuous autoregressive (CAR) models to analyze temperature data at Stockholm; and Härdle & Cabrera [25] also applied the CAR approach to Berlin temperature data, but they considered a nonzero market price of risk (MPR). To date no significant research for Korean weather derivatives and pricing has been reported, and a weather market has yet to be introduced. However, in order to keep pace with the growth of world-wide weather markets, the Financial Supervisory Commission of Korea now seems to favour the introduction and development of weather derivatives. The Korea Meteorological Administration (KMA) has also recently announced it intends to develop a weather index effective from 2012, to serve as one basic reference.

In this chapter we analyze the Seoul temperature data and then price related weather options, using the approach adopted in Refs. [2], [5] and [25]. This chapter is organized as follows. In Section 3.2, we construct our Seoul temperature model based on observed data. Put and call options are then priced in Section 3.3, based on temperature derivatives. Finally, in Section 3.4 the market price of risk (MPR) is calculated, using the Korea Composite Stock Price Index (KOSPI).

Table 3.1 Weather product: Temperature on CME (December, 2012).

	Product name	Region
U.S	U.S. Cooling (Monthly/Seasonal)	Atlanta, Chicago, Cincinnati
	U.S. Heating (Monthly/Seasonal)	New York, Dallas, Philadelphia
	U.S. Weekly Weather	Las Vegas, Boston, Houston, etc.
Canada	Canada CAT (Monthly/Seasonal)	Calgary, Edmonton
	Canada Cooling (Monthly/Seasonal)	Montreal, Toronto
	Canada Heating (Monthly/Seasonal)	Vancouver, Winnipeg
Europe	Europe CAT (Monthly/Seasonal)	London, Paris, Amsterdam, Berlin
	Europe Heating (Monthly/Seasonal)	Stockholm, Essen, Barcelona, Rome, etc.
Australia	Australia Cooling (Monthly/Seasonal)	Bankstown, Sydney
	Australia Heating (Monthly/Seasonal)	Brisbane Aero, Melbourne
Asia-Pacific	Asia-Pacific (Monthly/Seasonal)	Hiroshima, Osaka, Tokyo

Table 3.2 Weather product on CME (December, 2012).

Index	Product name	Region
Hurricanes	Hurricane	Gulf Coast, Florida, Southern Atlantic Coast
	Hurricane Seasonal	Northern Atlantic Coast, Eastern U.S.
	Hurricane Seasonal Maximum	Cat-In-A-Box, Florida Gold Coast
Frost	Frost (Monthly/Seasonal)	
Snowfall	Snowfall (Monthly/Seasonal)	Boston, New York Central Park, Chicago, etc.
Rainfall	Rainfall (Monthly/Seasonal)	Chicago O'Hare International Airport

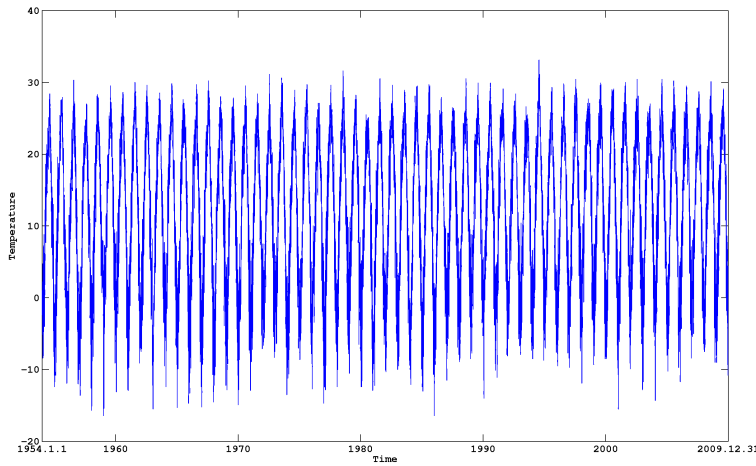

Figure 3.1 Daily average temperature from 1954.01.01to 2009.12.31 at Seoul, Korea.

3.2 Modelling of Seoul temperature

We investigate the temperature data for Seoul in a somewhat different way from previous analyses for other places. Firstly, most researchers [2, 3, 5, 6, 16, 25] have defined the daily mean temperature as the average of the maximum and minimum temperatures for that day, but we adopt the following definition for the daily average temperature.

Definition 3.2.1 (Daily average temperature (DAT))**.** *From the year 1997, the* ***daily average temperature*** T_t *is defined to be the average temperature of 8 observed temperature values at the 03, 06, 09, 12, 15, 18, 21, 24 hour times during the day* t*; and before 1997,* T_t *is defined as the average temperature of 4 observed values at the 03, 09, 15, 21 hour times during the day* t*.*

We begin with the 20440 DAT data recorded for the 56 years from 1954.01.01 to 2009.12.31 at Seoul, Korea (Fig. 3.1) obtained from the KMA [44]. Leap-year day data are excluded. These data, which basically contain seasonal periodic-

ity and an increment trend due to global warming, are to be interpreted as a function in time in the mathematical analysis. It seems natural to try to fit the yearly periodicity with a cosine polynomial and the global warming property with a linear term [2, 5, 25]. However, we assume

$$\Lambda_t = \lambda_0 + \lambda_1 t + \lambda_2 \cos \frac{2\pi(t - \lambda_3)}{365} + \lambda_4 \cos \frac{4\pi(t - \lambda_5)}{365} \ , \qquad (3.1)$$

and remark that the difference between the form used by Benth *et al* [5] and Eq. (3.1) is the fourth term representing a half-year period. We include this term so that the ACF analysis in Section 3.3.2 works when seasonality in the squared residuals remains apparent, as will be seen in Fig. 3.8(d). This seasonality is a distinct feature of the temperature at Seoul, compared to the other cities that have been considered elsewhere [2, 5, 7, 25].

Using the method of least squares, we get the coefficients $\lambda_0 = 11.1897$, $\lambda_1 = 0.0001$, $\lambda_2 = 13.9112$, $\lambda_3 = -161.2643$, $\lambda_4 = 1.3705$, and $\lambda_5 = -92.7957$. The fitted function and DAT are plotted in Fig. 3.2(a). The blue line is the daily average temperature, while the red one is a fitted form using Eq. (3.1). Fig. 3.2(b) also depicts these data and fitted function, during the 10 years from 2000.1.1 to 2009.12.31. The coefficient λ_2 represents half of the temperature difference between the highest DAT in summer and the lowest DAT in winter, which is approximately $28°C$ — cf. Table 3.3. Compared to European cities (Berlin [25] and Stockholm [2]) and other Asian cities (Tokyo, Osaka, Taipei [7]), this value is much higher. The second term in Eq. evidently reflects the greenhouse effect, with the annual average temperature rising as seen in Table 3.4.

Table 3.3 Temperature differences between the highest DAT in summer and the lowest DAT in winter.

Seoul	Berlin	Stockholm	Tokyo	Osaka	Taipei
$27.8°C$	$19.6°C$	$20.8°C$	$20.7°C$	$23°C$	$13.6°C$

Table 3.4 Monthly average temperatures during the 1950-1959 and 2000-2009 decades.

	1	2	3	4	5	6	7	8	9	10	11	12	Annual
1950's	-4.3	-1.0	3.5	10.6	16.4	20.6	23.9	25.1	20.1	13.0	6.6	-0.5	**11.2**
2000's	-1.6	1.0	6.0	12.8	18.3	22.5	24.9	25.7	21.6	15.3	7.5	0.4	**12.9**

3.3 Temperature Derivatives

There are three types of temperature indices used at the CME – HDD, CDD and CAT. The HDD_n and CDD_n indices usually measure temperatures over a period starting from day u_1 to day u_n, with regard to heating and cooling when the DAT is below and above $18°C$, respectively. The CAT index accounts for the accumulated average temperature over day u_1, day $u_2, \cdots$, day u_n. Specifically, these three types are defined as follows:

$$\begin{aligned} HDD_n &= \sum_{i=1}^{n} \max\left(18 - T_{u_i}, 0\right), \\ CDD_n &= \sum_{i=1}^{n} \max\left(T_{u_i} - 18, 0\right), \\ CAT_n &= \sum_{i=1}^{n} T_{u_i}. \end{aligned}$$

As shown in Table 3.1, the HDD and CDD indices are used in the USA, Canada and Australia. In Europe, the CAT index substitutes for the CDD index utilizing the HDD–CDD parity — thus

$$CDD_n - HDD_n = CAT_n - 18n. \tag{3.2}$$

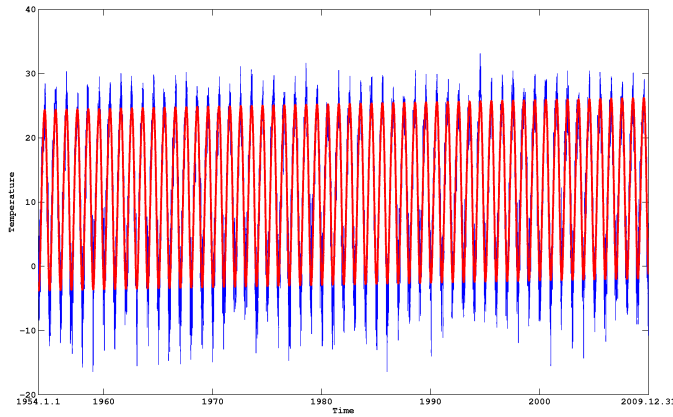

(a) 1954.01.01–2009.12.31

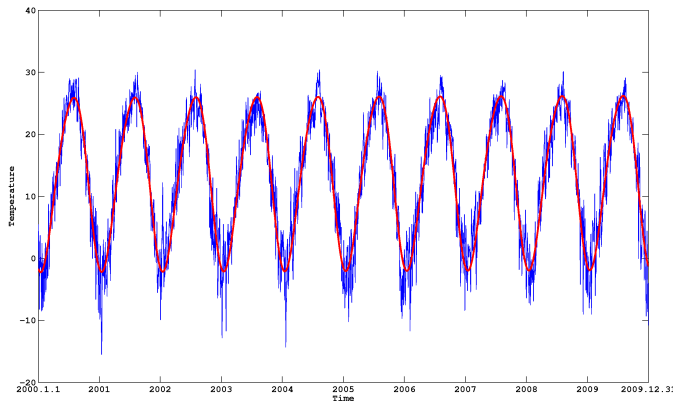

(b) 2000.01.01–2009.12.31

Figure 3.2 Seasonality effect and daily average temperatures for Seoul: the blue lines represent daily average temperatures (DAT), and the red lines fitted functions given by Eq. (3.1).

Similar to Japan, in Korea we may define the accumulated temperature index to be the sum over the period day u_1, day $u_2, \cdots$, day u_n of daily average temperatures, averaged over temperatures observed 8 times daily — i.e.

$$CAT_n = \sum_{i=1}^{n} T_{u_i} \ , \tag{3.3}$$

where $T_{u_i} = \sum_{j=1}^{8} \tilde{T}_{u_i,j}/8$ involves the temperature $\tilde{T}_{u_i,j}$ measured at hour $3j$ on day u_i, $j = 1, \cdots, 8$.

3.3.1 Option pricing for temperature derivatives 1: HDD and CDD

In order to calculate option pricing for the HDD and CDD, we follow the scheme of Alaton *et al.* [2] where the mean temperature T_t follows the Ornstein-Uhlenbeck process with mean reverting rate a — i.e.

$$dT_t = a(T_t^m - T_t)\, dt + \sigma_t\, dW_t \ , \tag{3.4}$$

where T_t^m is the equilibrium or mean temperature value given by the expected temperature at day t from the past historical data for the temperature. We normally choose $T_t^m = \Lambda_t$, where Λ_t is given by Eq. (3.1). In Eq. (3.4), σ_t represents the degree of volatility around T_t^m, and W_t the Brownian motion on the probability space $(\Omega, \mathcal{F}, P)$ with a filtration $\{\mathcal{F}_t\}$.

To satisfy a mean-reverting property, we should add the term dT_t^m/dt to Eq. (3.4) – cf. Dornier & Querel [16]. We then arrive at the stochastic differential equation

$$dT_t = \left\{ \frac{dT_t^m}{dt} + a(T_t^m - T_t) \right\} dt + \sigma_t\, dW_t \tag{3.5}$$

Table 3.5 The quadratic variation $\hat{\sigma}_\mu$ given by Eq. (3.7).

Jan.	Feb.	Mar.	Apr.	May	Jun.	Jul.	Aug.	Sep.	Oct.	Nov.	Dec.
3.079	2.718	2.404	2.356	2.139	1.758	1.592	1.472	1.540	2.036	2.887	3.143

with solution given by

$$T_t = (x - T_s^m)e^{-a(t-s)} + T_t^m + \int_s^t e^{-a(t-\tau)}\sigma_\tau \, dW_\tau \ , \tag{3.6}$$

where $x = T_s$ is the temperature observed at the starting day s. We need an estimation of both a and σ in Eq. (3.6). For $j = 1, \cdots, 365$, let $\overline{T}_j$ denote the average temperature of $DAT_{j+365(k-1)}$ where $k = 1, \cdots, 56$ – i.e. the average of all DAT's at the jth day of each year from 1954 to 2009. We then introduce an estimator σ based on the quadratic variation of T_t – i.e.

$$\hat{\sigma}_\mu = \sqrt{\frac{1}{N_\mu} \sum_{j=0}^{N_\mu - 1} \left(\overline{T}_{j+1+s_\mu} - \overline{T}_{j+s_\mu} \right)^2} \ , \tag{3.7}$$

where μ denotes a specific month ($\mu = 1, \cdots, 12$) of the year and N_μ the number of days in that month, and s_μ indicates the number of days up to the last day of the previous month $(\mu - 1)$.

Table 3.5 shows the quadratic variation $\hat{\sigma}_\mu$ of each month, where it is notable that the variations in winter are about twice as large as those in the summer. As previously noted, there are cycles of three cold days and four warm days during winter, and the hot temperature in summer does not change significantly – and such characteristic features in the Korean peninsula should be taken into account in modelling relevant weather derivatives and option pricing. With $\hat{\sigma}_\mu$ from Table 3.5, we obtain the mean-reversion parameter value $\hat{a}_n = 0.2748$, based on the martingale estimation functions method [8]

where

$$\hat{a}_n = \frac{\sum_{i=2}^{n} Y_{i-1}\Big\{T_i - T_{i-1} - dT_{i-1}^m/dt\Big\}}{\sum_{i=2}^{n} Y_{i-1}\{T_{i-1}^m - T_{i-1}\}}\,, \tag{3.8}$$

with $Y_{i-1} = (T_{i-1}^m - T_{i-1})/\overline{\sigma}_{i-1}^2$ $(i = 2, \cdots, n)$ and $\overline{\sigma}_j = \hat{\sigma}_k$ if the j-th day starting from 1 January 1954 lies in the k-th month in some year.

Considered a martingale measure Q, characterized by the market price of risk θ, the temperature satisfies the following stochastic differential equation:

$$dT_t = \left\{ \frac{dT_t^m}{dt} + a(T_t^m - T_t) - \theta\sigma_t \right\} dt + \sigma_t\, dW_t^\theta. \tag{3.9}$$

Proposition 3.3.1. *The solution of the above stochastic differential equation* (3.9) *can be represented by*

$$T_t = (x - T_s^m)e^{-a(t-s)} + T_t^m - \int_s^t \theta e^{-a(t-\tau)}\sigma_\tau\, d\tau + \int_s^t e^{-a(t-\tau)}\sigma_\tau\, dW_\tau,$$

where $x = T_s$ is the temperature observed at the starting day s.

Proof. Let $f(T_t, t) = T_t e^{at}$. Then,

$$\begin{aligned} df(T_t, t) &= e^{at}dT_t + aT_t e^{at}dt \\ &= e^{at}\left[\left\{ \frac{dT_t^m}{dt} + a(T_t^m - T_t) - \theta\sigma_t \right\} dt + \sigma_t\, dW_t\right] + aT_t e^{at}dt \\ &= e^{at}dT_t^m + ae^{at}T_t^m dt - \theta e^{at}\sigma_t dt + e^{at}\sigma_t\, dW_t. \end{aligned}$$

Integrating over $[s, t]$, one can get

$$T_t e^{at} - T_s e^{as} = e^{at}T_t^m - e^{as}T_s^m - \int_s^t \theta e^{a\tau}\sigma_\tau\, d\tau + \int_s^t e^{a\tau}\sigma_\tau\, dW_\tau,$$

and then,

$$T_t = T_t^m + (x - T_s^m)e^{-a(t-s)} - \int_s^t \theta e^{-a(t-\tau)}\sigma_\tau \, d\tau + \int_s^t e^{-a(t-\tau)}\sigma_\tau \, dW_\tau.$$

□

In order to price call and put options for the HDD, we first compute the conditional expectation and variance. Let us consider option prices under a martingale measure Q characterized by the MPR θ, which is equivalent to P. From the Girsanov theorem, the expectation changes under the measure Q but the variance does not. Therefore we have the following propositions.

Proposition 3.3.2 (Alaton *et al.* [2])**.** *Assume that the temperature T_t satisfies the stochastic differential equation* (3.9) *under a martingale measure Q. Then,*

$$\begin{aligned}
E^Q[T_{t_i}|\mathcal{F}_t] &= (T_t - T_t^m)e^{-a(t_i-t)} + T_{t_i}^m - \frac{\theta\sigma_i}{a}\Big(1 - e^{-a(t_i-t)}\Big) \,, \\
Var^Q[T_{t_i}|\mathcal{F}_t] &= \frac{\sigma_i^2}{2a}\Big(1 - e^{-2a(t_i-t)}\Big), \\
Cov^Q[T_{t_i}, T_{t_j}|\mathcal{F}_t] &= e^{-a(t_j-t_i)}\frac{\sigma_i^2}{2a}\Big(1 - e^{-2a(t_i-t)}\Big),
\end{aligned}$$

for $0 \le t \le t_i \le t_j$.

On setting

$$\beta_n = (K - \mu_n)/\gamma_n \,, \quad \mu_n = E^Q[HDD_n|\mathcal{F}_t] = 18n - \sum E^Q[T_{t_i}|\mathcal{F}_t], \quad (3.10)$$

where $\gamma_n^2 = Var^Q[HDD_n|\mathcal{F}_t]$, we find the price of the HDD call option given

Table 3.6 Option prices: Market Price of Risk (MPR)=0, $r = 0.036$, and the trading date is the first of December for the HDD and the first of July for the CDD, respectively.

Index	HDD call	HDD put	CDD call	CDD put
Strike price	600	600	220	220
Measurement Period	Jan. 2011	Jan. 2011	Aug. 2011	Aug. 2011
Price	23.25	16.25	9.97	8.75

by

$$\begin{aligned} HDD_{call}(t) &= \exp\left[-r(t_n - t)\right] E^Q\Big[\max\left(HDD_n - K, 0\right)|\mathcal{F}_t\Big] \\ &= \exp\left[-r(t_n - t)\right]\left((\mu_n - K)\Phi(-\beta_n) + \frac{\gamma_n}{\sqrt{2\pi}}\exp\Big(-\frac{\beta_n^2}{2}\Big)\right), \end{aligned} \tag{3.11}$$

where Φ is the cumulative distribution function for the standard normal distribution. Further, the price of the HDD put option is likewise given by

$$\begin{aligned} HDD_{put}(t) &= \exp\left[-r(t_n - t)\right] E^Q[\max\left(K - HDD_n, 0\right)|\mathcal{F}_t] \\ &= \exp\left[-r(t_n - t)\right]\left[(K - \mu_n)\left(\Phi(\beta_n) - \Phi\Big(-\frac{\mu_n}{\gamma_n}\Big)\right)\right. \\ &\qquad \left. + \frac{\gamma_n}{\sqrt{2\pi}}\left(\exp\Big(-\frac{\beta_n^2}{2}\Big) - \exp\Big(-\frac{\mu_n^2}{2\gamma_n^2}\Big)\right)\right]. \end{aligned} \tag{3.12}$$

The formulae for CDD call and put options can be derived analogously, and are quite similar to Eqs. (3.11) and (3.12). It is notable that θ in Eq. (3.10) represents the market price of risk (MPR), discussed in detail in Section 3.4. From these equations, we get the option prices shown in Table 3.6, assuming that $\theta = 0$. The HDD and CDD call and put option prices with $r = 0.036$ are illustrated in Fig. 3.3, 3.9 for January and August of 2011, respectively.

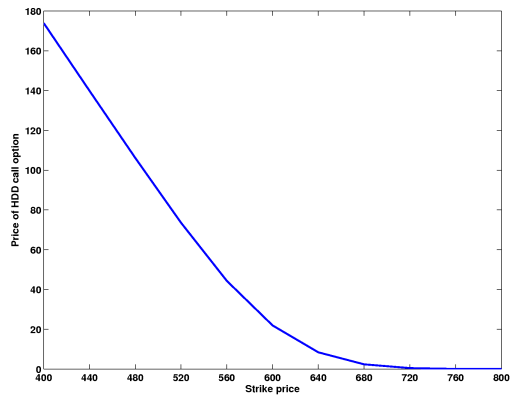

(a) HDD call

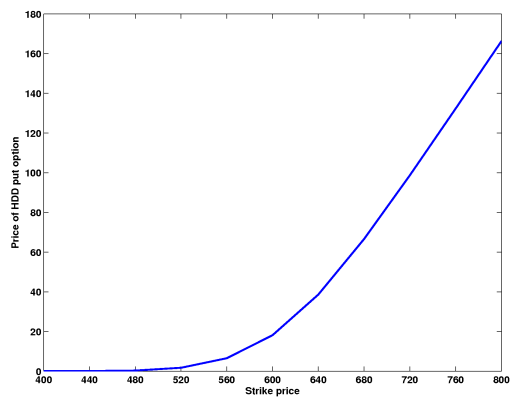

(b) HDD put

Figure 3.3 Option prices: Market Price of Risk (MPR) $= 0$, $r = 0.036$, for the HDD call and put options calculated for the months of January 2011. The measurement period is the entire month of January and the trading date is the first of December.

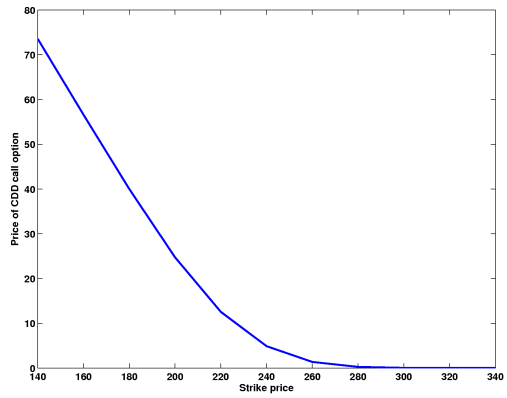

(a) CDD call

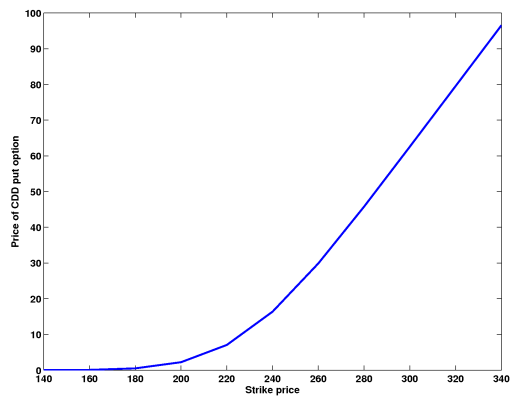

(b) CDD put

Figure 3.4 Option prices: Market Price of Risk (MPR) $= 0$, $r = 0.036$, for the CDD call and put options calculated for the months of August 2011. The measurement period is the entire month of August and the trading date is the first of July.

3.3.2 Option pricing for temperature derivatives 2: CAT

In this subsection, we estimate the CAT-futures price and its option value, using the Benth *et al.* [5] temperature dynamics model, continuous time AR models (CAR). Letting W_t denote the Brownian motion on the probability space $(\Omega, \mathcal{F})$ with a filtration $\{\mathcal{F}_t\}_{0\le t\le \tau_{\max}}$, we now consider the vectorial Ornstein-Uhlenbeck process

$$d\mathbf{X}_t = A\mathbf{X}_t\, dt + \mathbf{e}_p \sigma_t\, dW_t\ , \tag{3.13}$$

where $\mathbf{e}_k$ is the k-th unit vector in $\mathbb{R}^p,\ k = 1, \cdots, p.$ and A is the $p \times p$ matrix

$$A = \begin{bmatrix} 0 & 1 & 0 & \cdots & 0 \\ 0 & 0 & 1 & \cdots & 0 \\ \vdots & \vdots & \vdots & \ddots & \vdots \\ 0 & 0 & 0 & \cdots & 1 \\ -\alpha_p & -\alpha_{p-1} & -\alpha_{p-2} & \cdots & -\alpha_1 \end{bmatrix}.$$

Further, denoting by X_{qt} the q-th coordinate of the vector $\mathbf{X}_t, q = 1, \cdots, p$ we have

$$T_t = \Lambda_t + X_{1t}\ , \tag{3.14}$$

whence from Ito's lemma the temperature dynamic process is described as follows.

Lemma 3.3.3. *The stochastic process* $\mathbf{X}_t$ *in Eq.* (3.13) *can be expressed as*

$$\mathbf{X}_s = e^{A(s-t)}\mathbf{X}_t + \int_t^s e^{A(s-u)}\mathbf{e}_p \sigma_u\, dW_u\ ,$$

for $s \ge t \ge 0$.

We now proceed to consider the difference between the DAT and the seasonal behaviour

$$X_t = T_t - \Lambda_t \ . \tag{3.15}$$

The partial autocorrelation function (PACF) for X_t is plotted in Fig. 3.5, showing that the $AR(3)$-process [5] is suitable for the analysis of our data. The fitted autoregressive process using MATLAB corresponds to

$$X_{t+3} = 0.9385X_{t+2} - 0.3472X_{t+1} + 0.1132X_t + \sigma_t\epsilon_t \ , \tag{3.16}$$

where the seasonal variance σ_t^2 and the residual ϵ_t are computed as follows.

We first compute the residuals $\hat{\epsilon_t} = X_{t+3} - 0.9385X_{t+2} + 0.3472X_{t+1} - 0.1132X_t$, as plotted in Figs. 3.6(a) and 3.6(b) together with their squares $\hat{\epsilon_t}^2$. The ACF of the residuals and the squared residuals of AR(3) are plotted in Figs. 3.8(a) and 3.8(c), showing that the residuals are close to zero but the squared residuals exhibit a high seasonality pattern. To avoid this problem, we consider the seasonal variance function σ_t^2 in Eq. (3.17). We also use the least squares method to get the parameters c_j's in the following formula:

$$\sigma_t^2 = c_1 + \sum_{j=1}^{4}\left(c_{2j}\cos\frac{2j\pi t}{365} + c_{2j+1}\sin\frac{2j\pi t}{365}\right) \ , \tag{3.17}$$

where $c_1 = 4.4823$, $c_2 = 2.5635$, $c_3 = 0.7150$, $c_4 = 0.8952$, $c_5 = -0.5473$, $c_6 = 0.3197$, $c_7 = -0.3531$, $c_8 = -0.1315$ and $c_9 = -0.0055$. After dividing $\hat{\epsilon_t}^2$ by the seasonal variance function σ_t^2, as shown in Fig. 3.8(d) we find that the plot of the squared residuals results in much smaller values than before – and moreover, it presents a non-seasonal pattern.

For $p = 1$, $\mathbf{X}_t = X_{1t}$ and $dX_{1t} = -\alpha_1 X_{1t}\,dt + \sigma_t\,dW_t$, and for $p = 2$, $X_{1(t+2)} \approx (2-\alpha_1)X_{1(t+1)} + (\alpha_1 - \alpha_2 - 1)X_{1t} + \sigma_t(W_{t+1} - W_t)$. And by the

finite difference approximation,

$$\begin{aligned} X_{1(t+3)} &\approx (3-\alpha_1)X_{1(t+2)} + (2\alpha_1 - \alpha_2 - 3)X_{1(t+1)} \\ &\quad +(\alpha_2 + 1 - \alpha_1 - \alpha_3)X_{1t} + \sigma_t(W_{t+1} - W_t), \end{aligned} \tag{3.18}$$

for $p = 3$. Consequently, using the equation (3.18) we obtained values for the coefficients of CAR(3) – $\alpha_1 = 2.0615$, $\alpha_2 = 1.4701$, $\alpha_3 = 0.2955$ (cf. Benth *et al.* [5]).

Here, we assume that all equivalent measures Q will be risk-neutral probabilities. To compute arbitrage free price of temperature, we consider a parametrized class of a risk-neutral probability measure Q, i.e. $W_t^\theta = W_t - \int_0^t \theta_u du$. Here θ represents the market price of risk. By Girsanov theorem, W_t is a Brownian motion. And the stochastic process under Q_θ is given by

$$d\mathbf{X}_t = (A\mathbf{X}_t + \mathbf{e}_p\sigma_t\theta_t)dt + \mathbf{e}_p\sigma_t\, dW_t^\theta\ . \tag{3.19}$$

The futures price for the CAT with the temperature measurement period $[\tau_1, \tau_2]$ is

$$F_{CAT(t,\tau_1,\tau_2)} = E^{Q_\theta}\left[\int_{\tau_1}^{\tau_2} T_s ds \big| \mathcal{F}_t\right]\ , \tag{3.20}$$

where the price of the futures $F_{CAT(t,\tau_1,\tau_2)}$ is $\mathcal{F}_t$-adapted.

In Benth *et al.* [5], explicit formulae for the CAT futures price and the call option price are as given in the following Propositions:

Proposition 3.3.4 (Benth *et al.* [5])**.** *For $0 \le t \le \tau_1 < \tau_2$, the CAT futures price is*

$$\begin{aligned} F_{CAT(t,\tau_1,\tau_2)} &= \int_{\tau_1}^{\tau_2} \Lambda_u\, du + \mathbf{a}_{t,\tau_1,\tau_2}\mathbf{X}_t + \int_t^{\tau_1} \theta_u\sigma_u\mathbf{a}_{t,\tau_1,\tau_2}\mathbf{e}_p\, du \\ &\quad + \int_{\tau_1}^{\tau_2} \theta_u\sigma_u\mathbf{e}_1^T A^{-1}\Big[\exp[A(\tau_2 - u)] - I_p\Big]\mathbf{e}_p\, du\ , \end{aligned}$$

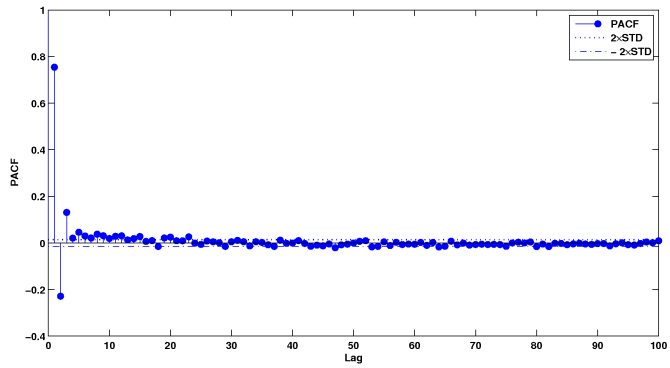

Figure 3.5 Partial autocorrelation function (PACF) for X_t during 1954.01.01 to 2009.12.31.

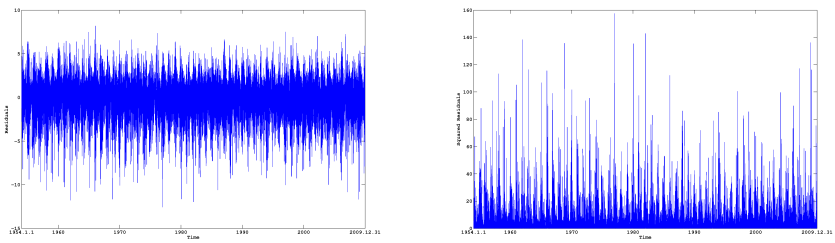

(a) Residuals (b) Squared residuals

Figure 3.6 Residuals $\hat{\epsilon}_t$ and squared residuals ${\hat{\epsilon}_t}^2$ for the AR(3) during 1954.01.01 to 2009.12.31.

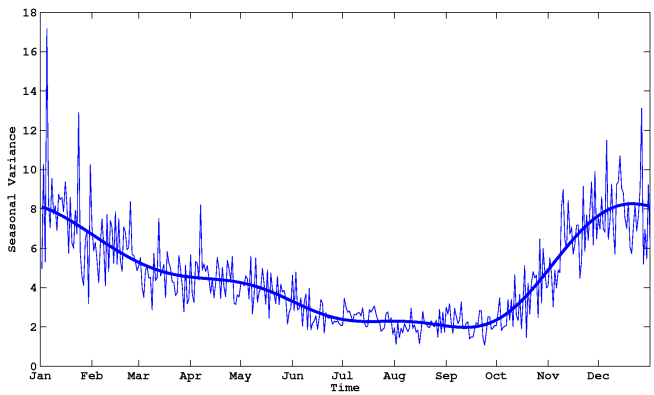

Figure 3.7 Seasonal variance: daily empirical variance and fitted squared volatility function, represented by the smoothed curve.

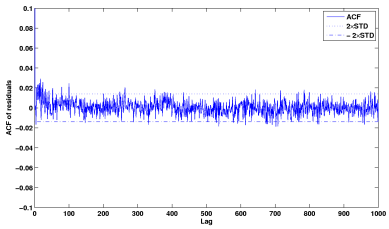

(a) Residuals

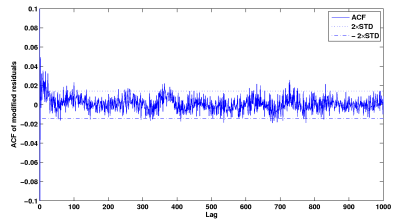

(b) Residuals after

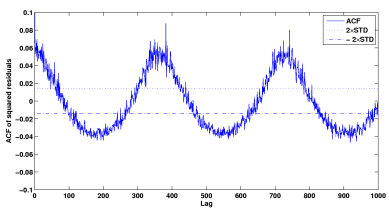

(c) Squared residuals

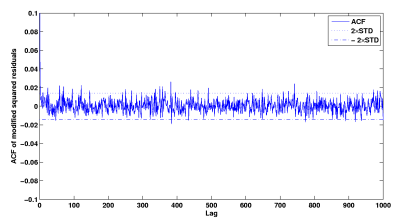

(d) Squared residuals after

Figure 3.8 ACF Residuals $\hat{\epsilon}_t$ and squared residuals $\hat{\epsilon}_t{}^2$ for the AR(3) during the period 1954.01.01 to 2009.12.31.

Table 3.7 *CAT* call option prices: Market Price of Risk (MPR)= 0, $r = 0.036$, and the measurement period the whole month of August, with the trading date the first of July.

Exercise time (τ)	K=650	K=700	K=750
25. August 2011	138.64	92.25	45.87
28. August 2011	137.40	91.43	45.46
31. August 2011	136.17	90.61	45.05

where $\mathbf{a}_{t,\tau 1,\tau 2} = \mathbf{e}_1' A^{-1}(\exp(A(\tau_2 - t)) - \exp(A(\tau_1 - t)))$.

Proposition 3.3.5 (Benth *et al.* [5])**.** *The price of the CAT call option at* $t \leq \tau$ *is*

$$\begin{aligned} C_{CAT(t,\tau,\tau_1,\tau_2)} &= \exp\left[-r(\tau - t)\right] \times \Big\{ \big(F_{CAT(t,\tau_1,\tau_2)} - K\big)\Phi(w(t,\tau,\tau_1,\tau_2)) \\ &\quad + \int_t^\tau \Sigma^2_{CAT}(s,\tau_1,\tau_2)\, ds\, \Phi'(w(t,\tau,\tau_1,\tau_2)) \Big\}, \end{aligned}$$

with the strike price K at the exercise time $\tau \leq \tau_1$, the measurement period $[\tau_1, \tau_2]$, and w and Σ_{CAT} given by

$$w(t, \tau, \tau_1, \tau_2) = \frac{F_{CAT(t,\tau_1,\tau_2)} - K}{\sqrt{\int_t^\tau \Sigma_{CAT}^2(s, \tau_1, \tau_2)\, ds}} ,$$
$$\Sigma_{CAT}(t, \tau_1, \tau_2) = \sigma(t)\mathbf{e}_1' A^{-1}(e^{A(\tau_2 - t)} - e^{A(\tau_1 - t)})\mathbf{e}_p .$$

3.4 Estimating the Market Price of Risk (MPR)

In Eq. (3.10) and Proposition 3.3.4, θ represents the market price of risk (MPR). Many researchers [11, 25, 27] have shown that the MPR has a significant effect on pricing options, so it must be determined to calculate the option prices for the HDD, CDD and CAT. In order to estimate the MPR value, information on the actual price for the weather derivatives would be needed if we were to proceed as Härdle & Cabrera [25] did to infer the MPR from the actual option price for Berlin – but in Korea there is no weather market. Consequently, we computed the MPR of the Korea Composite Stock Price Index (KOSPI), and used this value as the MPR for the Korean weather derivatives. Thus the assumed θ is

$$\theta = \frac{\mu - r}{\sigma} ,$$

where r is the risk-free rate, μ is the return, and σ the stock volatility. From the returns on stocks and on 3-year government bonds [17, 45], the estimation of the MPR from the KOSPI was -0.0029, and the absolute value of the MPR for temperature should be smaller [27].

Recalling that β_n and μ_n in Eq. (3.10) depend upon the MPR, we pro-

ceeded to obtain the value of θ to use in Eq. (3.10). In our calculations we used the three MPR values 0, -0.0029 and 0.0029, and evaluated the corresponding β_n and μ_n values (denoted by β_n^j and μ_n^j, $j = 0, -, +$) using $\theta = 0$, -0.0029 and 0.0029, respectively. Fig. 3.9 shows the dependency of the HDD and CDD option prices on the MPR.

Remark 3.4.1. *For the HDD call option, we get the inequalities $\mu_n^- < \mu_n^0 < \mu_n^+$, $\beta_n^+ < \beta_n^0 < \beta_n^-$ and $\mu_n^- - K < \mu_n^0 - K < \mu_n^+ - K$ in Section 3.1; the inequality $HDD_{call}^- < HDD_{call}^0 < HDD_{call}^+$ follows because Φ and the exponential function are monotonic increasing functions – cf. Fig. 3.9(a). The CDD call option is quite similar. Thus since $\mu_n = \sum E^Q[T_{t_i}|\mathcal{F}_t] - 18n$ for the CDD, we obtain $\mu_n^+ < \mu_n^0 < \mu_n^-$, $\beta_n^- < \beta_n^0 < \beta_n^+$ and $\mu_n^+ - K < \mu_n^0 - K < \mu_n^- - K$ such that $CDD_{call}^+ < CDD_{call}^0 < CDD_{call}^-$ – cf. Fig. 3.9(c).*

Tables 3.8 and 3.9 show the prices of CAT call options based on Propositions 3.3.4 and 3.3.5 with nonzero MPR. These results imply that the option prices depend on both the exercise time and the MPR, decreasing as the measurement period gets closer or when the MPR is larger.

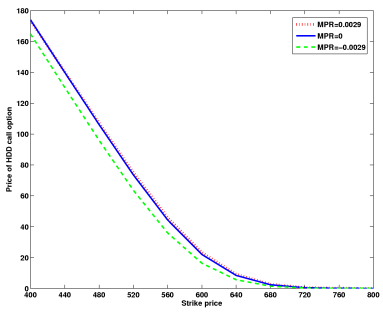

(a) HDD call

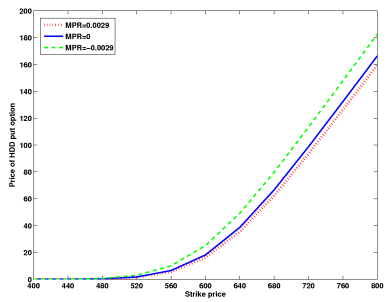

(b) HDD put

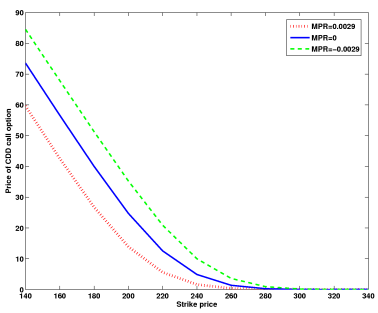

(c) CDD call

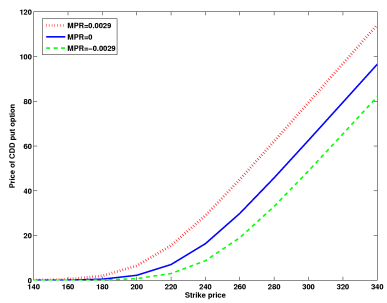

(d) CDD put

Figure 3.9 Option prices. For $r = 0.036$, The calculated HDD and CDD options for the months of January and August 2011, respectively – the measurement period is the whole month of August, with the trading date being the first of July.

Table 3.8 CAT call option prices: Market Price of Risk (MPR)=0.0029, $r = 0.036$, and the measurement period the whole month of August, with the trading date the first of July.

Exercise time (τ)	$K = 650$	$K = 700$	$K = 750$
25. August 2011	139.06	92.68	46.29
28. August 2011	137.82	91.85	45.87
31. August 2011	136.58	91.02	45.46

Table 3.9 CAT call option prices. Market Price of Risk (MPR)=-0.0029, $r = 0.036$, and the measurement period is the whole month of August, with the trading date the first of July.

Exercise time (τ)	$K = 650$	$K = 700$	$K = 750$
25. August 2011	138.22	91.83	45.44
28. August 2011	136.98	91.01	45.04
31. August 2011	135.75	90.19	44.63

Chapter 4

Pricing Weather Derivatives using Laplace Transform Methods

4.1 Pricing option for weather sensitive asset

In [18] they derived PDEs for pricing option of weather sensitive asset with assumption that the asset price is a deterministic function of temperature. Let $x(t)$ be the asset price at time t, and T_t the temperature at t. Here we also consider the Ornstein-Uhlenbeck process with mean reverting rate $a > 0$,

$$dT_t = a(\mu - T_t)dt + \sigma dW_t, \tag{4.1}$$

where μ is mean temperature value and W_t is the Brownian motion.

Theorem 4.1.1 (Filar *et al.* [18])**.** *Assume that the temperature T_t follows the Ornstein-Uhlenbeck process* (4.1) *and the weather sensitive asset x is given by a quadratic form or exponential function of the temperature T_t. For risk-free*

interest rate r, the option price $u(x,t)$ of the weather sensitive asset x is as follows:

(i) Quadratic form: $x = T_t^2$,

$$\frac{\partial u}{\partial t} - rx\frac{\partial u}{\partial x} - 2\sigma^2 x\frac{\partial^2 u}{\partial x^2} + ru = 0, \tag{4.2}$$

(ii) Exponential form: $x = e^{-aT_t}$

$$\frac{\partial u}{\partial t} - rx\frac{\partial u}{\partial x} - \frac{1}{2}a^2\sigma^2 x^2\frac{\partial^2 u}{\partial x^2} + ru = 0, \tag{4.3}$$

for $(x,t) \in (0,\infty) \times (0,T]$.

Note that both PDEs (4.2), (4.3) are similar with the Black-Scholes equation. Following [1, 33], we can analyze the solvability of the Laplace transformed equation of the above PDEs. Here we focus on the equation (4.3) in the case of a European put option. Taking the Laplace transform of (4.3), the following equation is given

$$z\hat{u} - rx\frac{\partial \hat{u}}{\partial x} - \frac{1}{2}a^2\sigma^2 x^2\frac{\partial^2 \hat{u}}{\partial x^2} + r\hat{u} = u_0, \quad (x,z) \in \mathbb{R}_+ \times \Gamma. \tag{4.4}$$

Following the notation in [33], we denote the weighted Sobolev space V.

Definition 4.1.2 (The weighted Sobolev space)**.**

$$V = \{v \in L^2(\mathbb{R}_+) | x\frac{\partial v}{\partial x} \in L^2(\mathbb{R}_+)\},$$

The semi-norm and norm are given by

$$|v|_V = \Big(\int_0^\infty \Big|x\frac{\partial v}{\partial x}\Big|^2 dx\Big)^{1/2}, \quad ||v||_V = \Big(\int_0^\infty |v|^2 + \Big|x\frac{\partial v}{\partial x}\Big|^2 dx\Big)^{1/2}.$$

The Laplace transformed equation (4.4) can be given the following variational formulation: For each $z \in \Gamma$,

$$\text{Find } \hat{u} \in V \text{ such that } a_z(\hat{u}, v) = (u_0, v) \quad \forall v \in V, \tag{4.5}$$

where

$$\begin{aligned} a_z(u,v) = z(u,v) \quad &+ \quad \frac{1}{2}\int_0^\infty a^2\sigma(x)^2x^2\frac{\partial u}{\partial x}\frac{\partial \bar{v}}{\partial x}dx \\ &+ \quad \int_0^\infty \big(-r(x) + a^2\sigma(x)^2 + xa\sigma(x)\frac{\partial \sigma}{\partial x}\big)x\frac{\partial u}{\partial x}\bar{v}dx + \int_0^\infty r(x)u\bar{v}dx. \end{aligned}$$

Assumption 4.1.3. *Assume that σ is sufficiently regular. Moreover, we assume that*

1. *There exists positive constants, $\underline{\sigma}, \bar{\sigma}$ such that for all $x \in \mathbb{R}_+$,*

$$0 < \underline{\sigma} \leq \sigma(x) \leq \bar{\sigma}.$$

2. *There exists a positive constants, C_σ such that*

$$\left| x\frac{\partial \sigma}{\partial x} \right| \leq C_\sigma.$$

Under Assumption 4.1.3, one can obtain the following results which are similar with those in [33].

Lemma 4.1.4. *Under Assumption 4.1.3, the bilinear form a_z is continuous.*

Proof. If $u, v \in V$, then

$$\begin{aligned}
\Big|\frac{1}{2}\int_0^\infty a^2\sigma(x)^2x^2\frac{\partial u}{\partial x}\frac{\partial \bar{v}}{\partial x}dx\Big| &\leq \frac{a^2\bar{\sigma}^2}{2}|u|_V|v|_V,\\
\Big|\int_0^\infty \big(-r(x)+a^2\sigma(x)^2+xa\sigma(x)\frac{\partial\sigma}{\partial x}\big)x\frac{\partial u}{\partial x}\bar{v}dx\Big| &\leq 2(R+a^2\bar{\sigma}^2+C_\sigma a\bar{\sigma})|u|_V|v|_V,\\
\Big|\int_0^\infty (z+r(x))u\bar{v}dx\Big| &\leq (|z|+R)|u|_V|v|_V,
\end{aligned}$$

where $R = ||r||_{L^\infty(\mathbb{R}_+)}$. Hence, the bilinear form a_z is continuous. □

Lemma 4.1.5. *Under Assumption 4.1.3, there exist a constant $\lambda \geq 0$, which is independent of u and z, such that for all $u \in V$*

$$\Re\{a_z(u,u)\} \geq \frac{a^2\underline{\sigma}^2}{4}|v|_V^2 - (|z|+C)||u||^2_{L^2(\mathbb{R}_+)}.$$

Proof. If $u \in V$, then

$$\begin{aligned}
\Big|\frac{1}{2}\int_0^\infty a^2\sigma(x)^2x^2\frac{\partial u}{\partial x}\frac{\partial \bar{u}}{\partial x}dx\Big| &\geq \frac{a^2\underline{\sigma}^2}{2}|u|_V^2,\\
\Big|\int_0^\infty \big(-r(x)+a^2\sigma(x)^2+xa\sigma(x)\frac{\partial\sigma}{\partial x}\big)x\frac{\partial u}{\partial x}\bar{u}dx\Big| &\leq (R+a^2\bar{\sigma}^2+C_\sigma a\bar{\sigma})|u|_V||u||_{L^2(\mathbb{R}_+)}\\
&\leq \frac{a^2\underline{\sigma}^2}{4}|v|_V^2+\lambda||u||^2_{L^2(\mathbb{R}_+)},\\
\Big|\Re\{\int_0^\infty (z+r(x))u\bar{u}dx\}\Big| &\leq (|z|+R)||u||^2_{L^2(\mathbb{R}_+)},
\end{aligned}$$

where $\lambda = (R+a^2\bar{\sigma}^2+C_\sigma a\bar{\sigma})^2/(a\underline{\sigma})^2$, and $R = ||r||_{L^\infty(\mathbb{R}_+)}$. Using these inequalities, one can get

$$\Re\{a_z(u,u)\} \geq \frac{a^2\underline{\sigma}^2}{4}|v|_V^2 - (|z|+C)||u||^2_{L^2(\mathbb{R}_+)}.$$

□

Thus, by Lax-Milgram theorem, we obtain the following theorem.

Theorem 4.1.6. *Under Assumption 4.1.3, the weak problem* (4.5) *has a unique solution* $\hat{u} \in V$.

4.2 Pricing weather option using weather swaps

Here we consider another PDE which is dealt with swap. As shown by Jewson [28], the following PDE can be obtained.

Proposition 4.2.1 (Jewson [28])**.** *Assume that the swap is tradable without transaction cost and is used to delta hedge the option. With the swap price process,* $dS_t = rS_t dt + e^{r(t-T)} dW_t := rS_t dt + \sigma_s dW_t$, *the equation for weather swaps trading with premium* S *is given by*

$$\frac{\partial V}{\partial t} + \frac{1}{2} e^{2r(t-T)} \sigma^2 \frac{\partial^2 V}{\partial S^2} + rS \frac{\partial V}{\partial S} - rV = 0. \tag{4.6}$$

Proof. Suppose that we have the option, a short position Δ in premium, and an amount of cash cB invested in a risk-free bond B with interest rate r. Then, total value, Π is

$$\Pi = V - \Delta S + cB.$$

Here $V(S,t)$ is the option value, and Δ is the number of premium-based swaps, and B is the value of the bond. Then one gets

$$d\Pi = dV - \Delta dS - Sd\Delta + cdB + Bdc.$$

With the property of self-financing of the portfolio, it is written as

$$d\Pi = dV - \Delta dS + cdB,$$

and then it simplifies to

$$d\Pi = dV - \Delta dS + crBdt. \tag{4.7}$$

Applying Ito's lemme to $V(S,t)$, we obtain the following equation.

$$dV = \frac{\partial V}{\partial t}dt + \frac{\partial V}{\partial S}dS + \frac{1}{2}\sigma_s^2\frac{\partial^2 V}{\partial S^2}dt.$$

With the assumption of swap price process, one gets

$$dV = \Big(\frac{\partial V}{\partial t} + rS\frac{\partial V}{\partial S} + \frac{1}{2}\sigma_s^2\frac{\partial^2 V}{\partial S^2}\Big)dt + \Big(\sigma_s S\frac{\partial V}{\partial S}\Big)dW_t.$$

Inserting into (4.7), the change in the portfolio becomes

$$d\Pi = \Big(\frac{\partial V}{\partial t} + rS\frac{\partial V}{\partial S} + \frac{1}{2}\sigma_s^2\frac{\partial^2 V}{\partial S^2} - rS\Delta + crB\Big)dt + \Big(\sigma_s S\frac{\partial V}{\partial S} - \sigma_s\Delta\Big)dW_t. \tag{4.8}$$

Choosing Δ as $S\frac{\partial V}{\partial S}$, it is represented as

$$d\Pi = \Big(\frac{\partial V}{\partial t} + rS\frac{\partial V}{\partial S} + \frac{1}{2}\sigma_s^2\frac{\partial^2 V}{\partial S^2} - rS\Delta + crB\Big)dt. \tag{4.9}$$

Since the return on the portfolio have to be same to one on safe bonds, $d\Pi = \Pi r dt$. It gives

$$\Big(\frac{\partial V}{\partial t} + rS\frac{\partial V}{\partial S} + \frac{1}{2}\sigma_s^2\frac{\partial^2 V}{\partial S^2} - rS\Delta + crB\Big)dt = (V - \Delta S + cB)rdt,$$

and we then derive the equation (4.6). □

Since the equation (4.6) has time-dependent coefficients, Laplace transform method is not applicable directly. In order to deal with this problem, we consider the frozen coefficient method in [35].

The equation (4.6) can be rewritten in the form

$$\frac{\partial V}{\partial t} + (\alpha(t)A_1 + A_2)V = 0, \quad t \in (0, T], \tag{4.10}$$

where $\alpha(t)$ is time-dependent coefficient, A_1 and A_2 are spatial operators. We define $A(t) := \alpha(t)A_1 + A_2$ with $\alpha(t) = \frac{1}{2}e^{2r(t-T)}\sigma^2$, $A_1 = \frac{\partial^2}{\partial x^2}$, and $A_2 = rx\frac{\partial}{\partial x} - rI$. Following the notation used by Lee *et al.* [35], the following commutativeness can be easily checked,

$$A(t)(t\tilde{A}_t - s\tilde{A}_s) = (t\tilde{A}_t - s\tilde{A}_s)A(t) \qquad 0 \le s \le t \le T,$$

where $\tilde{A}_{t_0}(x) = \frac{1}{t_0}\int_0^{t_0} A(x, \tau)d\tau$. Given $t_0 \in (0, T]$, the problem (4.10) is reformulated to the following evolution problem which has a time-independent coefficient,

$$\frac{\partial V}{\partial t} + \tilde{A}_{t_0}V = 0, \quad t \in (0, T]. \tag{4.11}$$

One can then apply the Laplace transform method to solve (4.11).

Usually the time-marching methods and Monte Carlo simulation have been used for solving the equations (4.2), (4.3) and (4.6). To apply the Laplace transform method gives us more efficient results compared to other approaches.

Bibliography

[1] Y. Achdou and O. Pironneau. *Computational methods for option pricing.* Siam, Philadelphia, 2005.

[2] P. Alaton, B. Djehiche, and D. Stillberger. On modelling and pricing weather derivatives. *Appl. Math. Finance*, 9(1):1–20, 2002.

[3] F. Benth. On arbitrage-free pricing of weather derivatives based on fractional Brownian motion. *Appl. Math. Finance*, 10(4):303–324, 2003.

[4] F. Benth and J. S. Benth. The volatility of temperature and pricing of weather derivatives. *Quant. Finance*, 7:553–561, 2007.

[5] F. Benth, J. S. Benth, and S. Koekebakker. Putting a price on temperature. *Scand. J. Stat.*, 34:746–767, 2007.

[6] F. Benth, J. S. Benth, and S. Koekebakker. Stochastic modelling of electricity and related markets. *World Scientific Publishing*, 2008.

[7] F. Benth, W. K. Härdle, and B. López Cabrera. Pricing of asian temperature risk. *SFB 649 Discussion Paper 2009-046, Humboldt-Universität zu Berlin*, 2009.

[8] B. M. Bibby and M. Sorensen. Martingale estimation functions for discretely observed diffusion processes. *Bernoulli*, 1(1/2):017–039, 1995.

[9] D. C. Brody, J. Syroka, and M. Zervos. Dynamical pricing of weather derivatives. *Quant. Finance*, 3:189–198, 2002.

[10] T. J. I. Bromwich. Normal coordinates in dynamical systems. *Proc. Lond. Math. Soc.*, 15:401–448, 1916.

[11] M. Cao and J. Wei. Weather derivatives valuation and market price of weather risk. *J. Futures Markets*, 24:1065–1089, 2004.

[12] C.-C. Chang, J.-B. Lin, and W.-M. Shen. Pricing weather derivatives using a predicting power time series. *Asia-Pac. J. Financ. St.*, 38(6):863–890, 2009.

[13] CME. An introduction to CME weather products. *CME Alternative Investment Products*, 2005.

[14] B. Davies and B. Martin. Numerical inversion of the Laplace transform: A survey and comparison of methods. *J. Comput. Phys.*, 33(1):1–32, 1979.

[15] P.J Davies and P. Rabinowitz. *Methods of numerical integration*. Academic, New York, 1975.

[16] F. Dornier and M. Querel. Caution to the wind. *Energy Power Risk Management, Weather Risk Special Report*, pages 30–32, 2000.

[17] Korea Exchange. http://www.krx.co.kr. (accessed Mar. 6, 2011).

[18] J. Filar, B. Kang, and M. Korolkiewicz. Pricing financial derivatives on weather sensitive assets. *QFRC Research paper 223, University of Technology, Sydney*, 2008.

[19] H. Fujiwara. http://www-an.acs.i.kyoto-u.ac.jp/∼fujiwara/exflib.

[20] H. Fujiwara. Numerical real inversions of the Laplace transform and their applications. *RIMS Kokyuroku*, 1618:192–209, 2008.

[21] I. P. Gavrilyuk and V. L. Makarov. An exponentially convergent algorithm for nonlinear differential equations in Banach spaces. *Math. Comp.*

[22] I. P. Gavrilyuk and V. L. Makarov. Exponentially convergent parallel discretization method for the first order evolution equations. *Comput. Methods Appl. Math.*, 1:333–355, 2001.

[23] I. P. Gavrilyuk and V. L. Makarov. Exponentially convergent algorithms for the operator exponential with applications to inhomogeneous problems in Banach spaces. *SIAM J. Numer. Anal.*, 43(5):2144–2171, 2005.

[24] L. L. Golden, M. Wang, and C. Yang. Handling weather related risks through the financial markets: Considerations of credit risk, basis risk, and hedging. *J. Risk Insur.*, 74(2):319–346, 2007.

[25] W. K. Härdle and B. López Cabrera. Implied market price of weather risk. *SFB 649 Discussion Paper 2009-001, Humboldt-Universität zu Berlin*, 2009.

[26] G. Hertzler. Adapting to climate change and managing climate risks by using real options. *Aust. J. Agr. Res.*, 58(10):985–992, 2007.

[27] H. Huang, Y. Shiu, and P. Lin. HDD and CDD option pricing with market price of weather risk for Taiwan. *J. Futures Markets*, 28:790–814, 2008.

[28] S. Jewson and A. Brix. *Weather Derivative Valuation.* Cambridge, UK, 2005.

[29] T. Kanamura and K. Ohashi. Pricing summer day options by good–deal bounds. *Energ. Econ.*, 31(2):289–297, 2009.

[30] J. Kim and D. Sheen. Roundoff error control on numerical laplace inversion. 2012. in preparation.

[31] J. Kim and D. Sheen. A unified framework to several numerical laplace inversion schemes. 2012. in preparation.

[32] J. Kim, D. Sheen, and Sungwon Shin. Option pricing of weather derivatives for seoul. *EAJAM*, 2(4):309–325, 2012.

[33] H. Lee and D. Sheen. Laplace transformation method for the Black-Scholes equation. *Int. J. Numer. Anal. Model.*, 6(4):642–658

[34] J. Lee. Economics of weather change. *SERI Economy Focus*, 278:1–22, 2010.

[35] J. Lee, H. Lee, and D. Sheen. Laplace transform method for parabolic problems with time-dependent coefficients. *SIAM J. Numer. Anal.*, 51(1):112–125, 2013.

[36] J. Lee and D. Sheen. An accurate numerical inversion of Laplace transforms based on the location of their poles. *Comput & Math. Applic.*, 48(10–11):1415–1423, 2004

[37] J. Lee and D. Sheen. A parallel method for backward parabolic problems based on the Laplace transformation. *SIAM J. Numer. Anal.*, 44:1466–1486, 2006.

[38] J.-H. Lee. A study on the valuation of the CDD/HDD weather options. *Asia-Pac. J. Financ. St.*, 31:229–255, 2002.

[39] M. Li. The impact of return nonnormality on exchange options. *J. Futures Markets*, 28(9):845–870, 2008.

[40] M. López-Fernández and C. Palencia. On the numerical inversion of the Laplace transform of certain holomorphic mappings. *Appl. Numer. Math.*, 51:289–303, 2004.

[41] M. López-Fernández, C. Palencia, and A. Schädle. A spectral order method for inverting sectorial Laplace transforms. *SIAM J. Numer. Anal.*, 44(3):1332–1350, 2006.

[42] W. Mclean, I. H. Sloan, and V. Thomée. Time discretization via Laplace transformation of an integro-differential equation of parabolic type. *Numerische Mathematik*, 102:497–522, 2006.

[43] J. Morrison. Managing weather risk. *Futures Industry*, Jan/Feb:26–29, 2009.

[44] Korea's national weather center. http://www.kma.go.kr. (accessed Nov. 25, 2010).

[45] Economic Statistics System of the Bank of Korea. http://ecos.bok.or.kr. (accessed Feb. 14, 2011).

[46] D. J. Richards, M. R. Manfredo, and D. R. Sanders. Pricing weather derivatives. *Am. J. Agr. Econ.*, 86(4):1005–1017, 2004.

[47] D. Sheen, I. H. Sloan, and V. Thomée. A parallel method for time-discretization of parabolic equations based on Laplace transformation and quadrature. *IMA J. Numer. Anal.*, 23(2):269–299, 2003.

[48] H. Stern. The application of weather derivatives to mitigate the financial risk of climate variability and extreme weather events. *Aust. Meteorol. Mag.*, 50(3):171–182, 2001.

[49] A. Talbot. The accurate numerical inversion of Laplace transforms. *J. Inst. Maths. Applics.*, 23:97–120, 1979.

[50] J. W. Taylor and R. Buizza. Density forecasting for weather derivative pricing. *Int. J. Forecasting*, 22(1):29–42, 2006.

[51] M. Tumpach and Z. Juhaszova. Option-based temperature derivatives as the instruments for elimination of weather risk impacts. *Ekon. Cas.*, 55(2):125–144, 2007.

[52] J. A. C. Weideman. Improved contour integral methods for parabolic PDEs. *IMA J. Numer. Anal.*

[53] J. A. C. Weideman. Optimizing Talbot's contours for the inversion of the Laplace transform. *SIAM J. Numer. Anal.*

[54] J. A. C. Weideman and L. N. Trefethen. Parabolic and hyperbolic contours for computing the Bromwich integra. *Math. Comp.*, 76(259):1341–1356 (electronic), 2007.

[55] S. Yoo. Weather derivatives and seasonal forecasts. *Asia-Pac. J. Financ. St.*, 33(4):213–246, 2004.

국문초록

본 논문에서는 역 라플라스 변환의 효율적인 계산 방법과 이 때 발생하는 반올림 오차 에러를 분석한다. 역 라플라스 변환의 수치 해법은 경로의 선택, 매개화 그리고 수치구적법의 세 가지 관점에서 살펴본다. 그리고 쌍곡선 경로에서 발생하는 역 라플라스 변환의 반올림 오차 에러를 분석한다. 또한 배정밀도 환경과 다중정밀도 환경에서 역 라플라스 변환의 수치적 계산을 하였으며, 다중정밀도 환경에서의 계산이 보다 효율적인 결과를 제공한다.

서울의 기온데이터를 분석하고 이와 관련된 날씨파생상품을 다룬다. 서울의 기온데이터는 이전의 연구에서 살펴본 도시와는 다른 특징을 지니는데 특히 계절적 변동이 뚜렷하게 나타난다. 날씨파생상품의 가격을 평가하기 위해 평균 기온 데이터의 결정 모형을 구성하고 시뮬레이션한다. 그리고 날씨파생상품과 관련된 편미분방정식의 효율적인 풀이를 위해 라플라스 변환 방법을 적용한다.

주요어: 라플라스 변환, 경로적분, 반올림 오차, 다중정밀도, 날씨파생상품
학번: 2010-30084